Formation and Collisional Evolution of Kuiper Belt Objects

Scott J. Kenyon
Smithsonian Astrophysical Observatory

Benjamin C. Bromley
University of Utah

David P. O'Brien and Donald R. Davis
Planetary Science Institute

This chapter summarizes analytic theory and numerical calculations for the formation and collisional evolution of Kuiper belt objects (KBOs) at 20–150 AU. We describe the main predictions of a baseline self-stirring model and show how dynamical perturbations from a stellar flyby or stirring by a giant planet modify the evolution. Although robust comparisons between observations and theory require better KBO statistics and more comprehensive calculations, the data are broadly consistent with KBO formation in a massive disk followed by substantial collisional grinding and dynamical ejection. However, there are important problems reconciling the results of coagulation and dynamical calculations. Contrasting our current understanding of the evolution of KBOs and asteroids suggests that additional observational constraints, such as the identification of more dynamical families of KBOs (like the 2003 EL_{61} family), would provide additional information on the relative roles of collisional grinding and dynamical ejection in the Kuiper belt. The uncertainties also motivate calculations that combine collisional and dynamical evolution, a "unified" calculation that should give us a better picture of KBO formation and evolution.

1. INTRODUCTION

Every year in the galaxy, a star is born. Most stars form in dense clusters of thousands of stars, as in the Orion nebula cluster (*Lada and Lada,* 2003; *Slesnick et al.,* 2004). Other stars form in small groups of 5–10 stars in loose associations of hundreds of stars, as in the Taurus-Auriga clouds (*Gomez et al.,* 1993; *Luhman,* 2006). Within these associations and clusters, most newly formed massive stars are binaries; lower-mass stars are usually single (*Lada,* 2006).

Large, optically thick circumstellar disks surround nearly all newly formed stars (*Beckwith and Sargent,* 1996). The disks have sizes of ~100–200 AU, masses of ~0.01–0.1 $M_\odot$, and luminosities of ~0.2–1 $L_\star$, where $L_\star$ is the luminosity of the central star. The masses and geometries of these disks are remarkably similar to the properties of the minimum mass solar nebula (MMSN), the disk required for the planets in the solar system (*Weidenschilling,* 1977b; *Hayashi,* 1981; *Scholz et al.,* 2006).

As stars age, they lose their disks. For solar-type stars, radiation from the opaque disk disappears in 1–10 m.y. (*Haisch et al.,* 2001). Many older stars have optically thin *debris disks* comparable in size to the opaque disks of younger stars but with much smaller masses, $\lesssim$1 $M_\oplus$, and luminosities, $\lesssim 10^3$ $L_\star$ (chapter by Moro-Martín et al.). The lifetime of this phase is uncertain. Some 100-m.y.-old stars have no obvious debris disk; a few 1–10-G.y.-old stars have massive debris disks (*Greaves,* 2005).

In the current picture, planets form during the transition from an optically thick protostellar disk to an optically thin debris disk. From the statistics of young stars in molecular clouds, the timescale for this transition, ~10^5 yr, is comparable to the timescales derived for the formation of planetesimals from dust grains (*Weidenschilling,* 1977a; *Youdin and Shu,* 2002; *Dullemond and Dominik,* 2005) and for the formation of lunar-mass or larger planets from planetesimals (*Wetherill and Stewart,* 1993; *Weidenschilling et al.,* 1997; *Kokubo and Ida,* 2000; *Nagasawa et al.,* 2005; *Kenyon and Bromley,* 2006). Because the grains in debris disks have short collision lifetimes, $\lesssim$1 m.y., compared to the ages of their parent stars, $\gtrsim$10 m.y., high-velocity collisions between larger objects must maintain the small grain population (*Aumann et al.,* 1984; *Backman and Paresce,* 1993). The inferred dust production rates for debris disks around 0.1–10-G.y.-old stars, ~10^{20} g yr^{-1}, require an initial mass in 1-km objects, M_i ~ 10–100 $M_\oplus$, comparable to the amount of solids in the MMSN. Because significant long-term debris production also demands gravitational stirring by an ensemble of planets with radii of 500–1000 km or larger (*Kenyon and Bromley,* 2004a; *Wyatt et al.,* 2005), debris

disks probably are newly formed planetary systems (*Aumann et al.,* 1984; *Backman and Paresce,* 1993; *Artymowicz,* 1997; *Kenyon and Bromley,* 2002b, 2004a,b).

Kuiper belt objects (KBOs) provide a crucial test of this picture. With objects ranging in size from 10–20 km to ~1000 km, the size distribution of KBOs yields a key comparison with theoretical calculations of planet formation (*Davis and Farinella,* 1997; *Kenyon and Luu,* 1998, 1999a,b). Once KBOs have sizes of 100–1000 km, collisional grinding, dynamical perturbations by large planets and passing stars, and self-stirring by small embedded planets, produce features in the distributions of sizes and dynamical elements that observations can probe in detail. Although complete calculations of KBO formation and dynamical evolution are not available, these calculations will eventually yield a better understanding of planet formation at 20–100 AU.

The Kuiper belt also enables a vital link between the solar system and other planetary systems. With an outer radius of ≥1000 AU (Sedna's aphelion) and a current mass of ~0.1 $M_\oplus$ (*Luu and Jewitt,* 2002; *Bernstein et al.,* 2004, chapter by Petit et al.), the Kuiper belt has properties similar to those derived for the oldest debris disks (*Greaves et al.,* 2004; *Wyatt et al.,* 2005). Understanding planet formation in the Kuiper belt thus informs our interpretation of evolutionary processes in other planetary systems.

This paper reviews applications of coagulation theory for planet formation in the Kuiper belt. After a brief introduction to the theoretical background in section 2, we describe results from numerical simulations in section 3, compare relevant KBO observations with the results of numerical simulations in section 4, and contrast the properties of KBOs and asteroids in section 5. We conclude with a short summary in section 6.

2. COAGULATION THEORY

Planet formation begins with dust grains suspended in a gaseous circumstellar disk. Grains evolve into planets in three steps. Collisions between grains produce larger aggregates that decouple from the gas and settle into a dense layer in the disk midplane. Continued growth of the loosely bound aggregates leads to planetesimals, gravitationally bound objects whose motions are relatively independent of the gas. Collisions and mergers among the ensemble of planetesimals form planets. Here, we briefly describe the physics of these stages and summarize analytic results as a prelude to summaries of numerical simulations.

We begin with a prescription for the mass surface density Σ of gas and dust in the disk. We use subscripts "d" for the dust and "g" for the gas and adopt

$$\Sigma_{d,g} = \Sigma_{0d,0g}\left(\frac{a}{40\ AU}\right)^{-n} \quad (1)$$

where a is the semimajor axis. In the MMSN, n = 3/2, $\Sigma_{0d} \approx$ 0.1 g cm^{-2}, and $\Sigma_{0d} \approx$ 5–10 g cm^{-2} (*Weidenschilling,* 1977b; *Hayashi,* 1981). For a disk with an outer radius of 100 AU, the MMSN has a mass of ~0.03 $M_\odot$, which is comparable to the disk masses of young stars in nearby star-forming regions (*Natta et al.,* 2000; *Scholz et al.,* 2006).

The dusty midplane forms quickly (*Weidenschilling,* 1977a, 1980; *Dullemond and Dominik,* 2005). For interstellar grains with radii, r ~ 0.01–0.1 μm, turbulent mixing approximately balances settling due to the vertical component of the star's gravity. As grains collide and grow to r ~ 0.1–1 mm, they decouple from the turbulence and settle into a thin layer in the disk midplane. The timescale for this process is ~10^3 yr at 1 AU and ~10^5 yr at 40 AU.

The evolution of grains in the midplane is uncertain. Because the gas has some pressure support, it orbits the star slightly more slowly than the Keplerian velocity. Thus, orbiting dust grains feel a headwind that drags them toward the central star (*Adachi et al.,* 1976; *Weidenschilling,* 1984; *Tanaka and Ida,* 1999). For meter-sized objects, the drag timescale at 40 AU, ~10^5 yr, is comparable to the growth time. Thus, it is not clear whether grains can grow by direct accretion to kilometer sizes before the gas drags them into the inner part of the disk.

Dynamical processes provide attractive alternatives to random agglomeration of grains. In ensembles of porous grains, gas flow during disruptive collisions leads to planetesimal formation by direct accretion (*Wurm et al.,* 2004). Analytic estimates and numerical simulations indicate that grains with r ~ 1 cm are also easily trapped within vortices in the disk (e.g., *de la Fuente Marcos and Barge,* 2001; *Inaba and Barge,* 2006). Large enhancements in the solid-to-gas ratio within vortices allows accretion to overcome gas drag, enabling formation of kilometer-sized planetesimals in 10^4–10^5 yr.

If the dusty midplane is calm, it becomes thinner and thinner until groups of particles overcome the local Jeans criterion — where their self-gravity overcomes local orbital shear — and "collapse" into larger objects on the local dynamical timescale, ~10^3 yr at 40 AU (*Goldreich and Ward,* 1973; *Youdin and Shu,* 2002; *Tanga et al.,* 2004). This process is a promising way to form planetesimals; however, turbulence may prevent the instability (*Weidenschilling,* 1995, 2003, 2006). Although the expected size of a collapsed object is the Jeans wavelength, the range of planetesimal sizes the instability produces is also uncertain.

Once planetesimals with r ~ 1 km form, gravity dominates gas dynamics. Long-range gravitational interactions exchange kinetic energy (dynamical friction) and angular momentum (viscous stirring), redistributing orbital energy and angular momentum among planetesimals. For 1-km objects at 40 AU, the initial random velocities are comparable to their escape velocities, ~1 m s^{-1} (*Weidenschilling,* 1980; *Goldreich et al.,* 2004). The gravitational binding energy (for brevity, we use energy as a shorthand for specific energy), $E_g \sim 10^4$ erg g^{-1}, is then comparable to the typical collision energy, $E_c \sim 10^4$ erg g^{-1}. Both energies are smaller than the disruption energy — the collision energy

needed to remove half the mass from the colliding pair of objects — which is $Q_D^* \sim 10^5$–10^7 erg g^{-1} for icy material (*Davis et al.,* 1985; *Benz and Asphaug,* 1999; *Ryan et al.,* 1999; *Michel et al.,* 2001; *Leinhardt and Richardson,* 2002; *Giblin et al.,* 2004). Thus, collisions produce mergers instead of debris.

Initially, small planetesimals grow slowly. For a large ensemble of planetesimals, the collision rate is $n\sigma v$, where n is the number of planetesimals, σ is the cross-section, and v is the relative velocity. The collision cross-section is the geometric cross-section, πr^2, scaled by the gravitational focusing factor f_g

$$\sigma_c \sim \pi r^2 f_g \sim \pi r^2 (1 + \beta (v_{esc}/e v_K)^2) \quad (2)$$

where e is the orbital eccentricity, v_K is the orbital velocity, v_{esc} is the escape velocity of the merged pair of planetesimals, and $\beta \approx 2.7$ is a coefficient that accounts for three-dimensional orbits in a rotating disk (*Greenzweig and Lissauer,* 1990; *Spaute et al.,* 1991; *Wetherill and Stewart,* 1993). Because $e v_K \approx v_{esc}$, gravitational focusing factors are small, and growth is slow and orderly (*Safronov,* 1969). The timescale for slow, orderly growth is

$$t_s \approx 30 \left(\frac{r}{1000 \text{ km}} \right) \left(\frac{P}{250 \text{ yr}} \right) \left(\frac{0.1 \text{ g cm}^{-2}}{\Sigma_{0d}} \right) \text{G.y.} \quad (3)$$

where P is the orbital period (*Safronov,* 1969; *Lissauer,* 1987; *Goldreich et al.,* 2004).

As larger objects form, several processes damp particle random velocities and accelerate growth. For objects with r ~ 1–100 m, physical collisions reduce particle random velocities (*Ohtsuki,* 1992; *Kenyon and Luu,* 1998). For larger objects with $r \gtrsim 0.1$ km, the smaller objects damp the orbital eccentricity of larger particles through dynamical friction (*Wetherill and Stewart,* 1989; *Kokubo and Ida,* 1995; *Kenyon and Luu,* 1998). Viscous stirring by the large objects excites the orbits of the small objects. For planetesimals with r ~ 1 m to r ~ 1 km, these processes occur on short timescales, $\lesssim 10^6$ yr at 40 AU, and roughly balance when these objects have orbital eccentricity e ~ 10^{-5}. In the case where gas drag is negligible, *Goldreich et al.* (2004) derive a simple relation for the ratio of the eccentricities of the large ("l") and the small ("s") objects in terms of their surface densities $\Sigma_{l,s}$ (see also *Kokubo and Ida,* 2002; *Rafikov,* 2003a,b,c,d)

$$\frac{e_l}{e_s} \sim \left(\frac{\Sigma_l}{\Sigma_s} \right)^\gamma \quad (4)$$

with $\gamma = 1/4$ to 1/2. Initially, most of the mass is in small objects. Thus $\Sigma_l/\Sigma_s \ll 1$. For $\Sigma_l/\Sigma_s \sim 10^{-3}$ to 10^{-4}, $e_l/e_s \approx 0.1$–0.25. Because $e_s v_K \ll v_{l,esc}$ gravitational focusing factors for large objects accreting small objects are large. Runaway growth begins.

Runaway growth relies on positive feedback between accretion and dynamical friction. Dynamical friction produces the largest f_g for the largest objects, which grow faster and faster relative to the smaller objects and contain an ever-growing fraction of the total mass. As they grow, these protoplanets stir the planetesimals. The orbital velocity dispersions of small objects gradually approach the escape velocities of the protoplanets. With $e_s v_K \sim v_{l,esc}$, collision rates decline as runaway growth continues (equations (2) and (4)). The protoplanets and leftover planetesimals then enter the oligarchic phase, where the largest objects — oligarchs — grow more slowly than they did as runaway objects but still faster than the leftover planetesimals. The timescale to reach oligarchic growth is (*Lissauer,* 1987; *Goldreich et al.,* 2004)

$$t_o \approx 30 \left(\frac{P}{250 \text{ yr}} \right) \left(\frac{0.1 \text{ g cm}^{-2}}{\Sigma_{0d}} \right) \text{m.y.} \quad (5)$$

For the MMSN, $t_o \propto a^{-3}$. Thus, collisional damping, dynamical friction and gravitational focusing enhance the growth rate by 3 orders of magnitude compared to orderly growth.

Among the oligarchs, smaller oligarchs grow the fastest. Each oligarch tries to accrete material in an annular "feeding zone" set by balancing the gravity of neighboring oligarchs. If an oligarch accretes all the mass in its feeding zone, it reaches the "isolation mass" (*Lissauer,* 1987; *Kokubo and Ida,* 1998, 2002; *Rafikov,* 2003a; *Goldreich et al.,* 2004)

$$m_{iso} \approx 28 \left(\frac{a}{40 \text{ AU}} \right)^3 \left(\frac{\Sigma_{0d}}{0.1 \text{ g cm}^{-2}} \right) M_\oplus \quad (6)$$

Each oligarch stirs up leftover planetesimals along its orbit. Smaller oligarchs orbit in regions with smaller Σ_l/Σ_s. Thus, smaller oligarchs have larger gravitational focusing factors (equations (2) and (4)) and grow faster than larger oligarchs (*Kokubo and Ida,* 1998; *Goldreich et al.,* 2004).

As oligarchs approach m_{iso}, they stir up the velocities of the planetesimals to the disruption velocity. Instead of mergers, collisions then yield smaller planetesimals and debris. Continued disruptive collisions lead to a collisional cascade, where leftover planetesimals are slowly ground to dust (*Dohnanyi,* 1969; *Williams and Wetherill,* 1994). Radiation pressure from the central star ejects dust grains with $r \lesssim 1$–10 μm; Poynting-Robertson drag pulls larger grains into the central star (*Burns et al.,* 1979; *Artymowicz,* 1988; *Takeuchi and Artymowicz,* 2001). Eventually, planetesimals are accreted by the oligarchs or ground to dust.

To evaluate the oligarch mass required for a disruptive collision, we consider two planetesimals with equal mass m_p. The center-of-mass collision energy is

$$Q_i = v_i^2/8 \quad (7)$$

where the impact velocity $v_i^2 = v^2 + v_{esc}^2$ (*Wetherill and Stewart,* 1993). The energy needed to remove half the combined mass of two colliding planetesimals is

$$Q_D^* = Q_b\left(\frac{r}{1\text{ cm}}\right)^{\beta_b} + \rho Q_g\left(\frac{r}{1\text{ cm}}\right)^{\beta_g} \quad (8)$$

where $Q_b r^{\beta_b}$ is the bulk (tensile) component of the binding energy and $\rho Q_g r^{\beta_g}$ is the gravity component of the binding energy (*Davis et al.,* 1985; *Housen and Holsapple,* 1990, 1999; *Holsapple,* 1994; *Benz and Asphaug,* 1999). We adopt $v \approx v_{esc,o}$, where $v_{esc,o} = (Gm_o/r_o)^{1/2}$ is the escape velocity of an oligarch with mass m_o and radius r_o. We define the disruption mass m_d by deriving the oligarch mass where $Q_i \approx Q_D^*$. For icy objects at 30 AU

$$m_d \sim 3 \times 10^{-6}\left(\frac{Q_D^*}{10^7\text{ erg g}^{-1}}\right)^{3/2} M_\oplus \quad (9)$$

Figure 1 illustrates the variation of Q_D^* with radius for several variants of equation (8). For icy objects, detailed numerical collision simulations yield $Q_b \lesssim 10^7$ erg g^{-1}, $-0.5 \lesssim \beta_b \lesssim 0$, $\rho \approx$ 1–2 g cm^{-3}, $Q_g \approx$ 1–2 erg cm^{-3}, and $\beta_g \approx$ 1–2 (solid line in Fig. 1) (*Benz and Asphaug,* 1999; see also chapter by Leinhardt et al.). Models for the breakup of Comet Shoemaker-Levy 9 suggest a smaller component of the bulk strength, $Q_b \sim 10^3$ erg g^{-1} (e.g., *Asphaug and Benz,* 1996), which yields smaller disruption energies for smaller objects (Fig. 1, dashed and dot-dashed curves). Because nearly all models for collisional disruption yield similar results for objects with $r \gtrsim 1$ km (e.g., *Kenyon and Bromley,* 2004d), the disruption mass is fairly independent of theoretical uncertainties once planetesimals become large. For typical $Q_D^* \sim 10^7$–10^8 erg g^{-1} for 1–10-km objects (Fig. 1), leftover planetesimals start to disrupt when oligarchs have radii $r_o >$ 200–500 km.

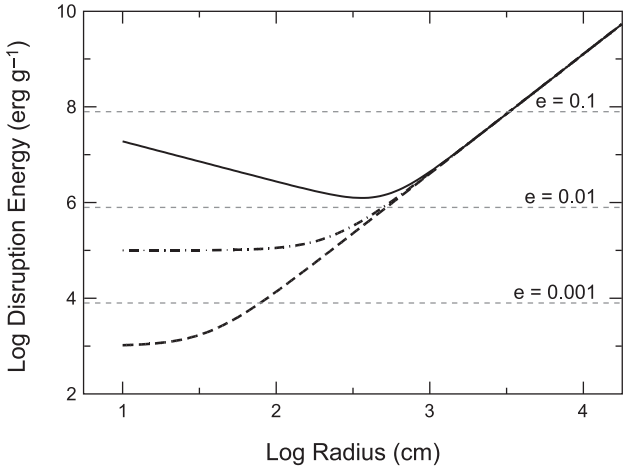

Fig. 1. Disruption energy, Q_D^*, for icy objects. The solid curve plots a typical result derived from numerical simulations of collisions that include a detailed equation of state for crystalline ice ($Q_b = 1.6 \times 10^7$ erg g^{-1}, $\beta_b = -0.42$, $\rho = 1.5$ g cm^{-3}, $Q_g = 1.5$ erg cm^{-3}, and $\beta_b = 1.25$) (*Benz and Asphaug,* 1999). The other curves plot results using Q_b consistent with model fits to comet breakups ($\beta_b \approx 0$; $Q_b \sim 10^3$ erg g^{-1}, dashed curve; $Q_b \sim 10^5$ erg g^{-1}, dot-dashed curve) (*Asphaug and Benz,* 1996). The dashed horizontal lines indicate the center of mass collision energy (equation (7)) for equal-mass objects with e = 0.001, 0.01, and 0.1. Collisions between objects with $Q_i \ll Q_D^*$ yield merged remnants; collisions between objects with $Q_i \gg Q_D^*$ produce debris.

Once disruption commences, the final mass of an oligarch depends on the timescale for the collisional cascade (*Kenyon and Bromley,* 2004a,b,d; *Leinhardt and Richardson,* 2005). If disruptive collisions produce dust grains much faster than oligarchs accrete leftover planetesimals, oligarchs with mass m_o cannot grow much larger than the disruption radius (maximum oligarch mass $m_{o,max} \approx m_d$). However, if oligarchs accrete grains and leftover planetesimals effectively, oligarchs reach the isolation mass before collisions and radiation pressure remove material from the disk (equation (6)) (*Goldreich et al.,* 2004). The relative rates of accretion and disruption depend on the balance between collisional damping and gas drag — which slow the collisional cascade — and viscous stirring and dynamical friction — which speed up the collisional cascade. Because deriving accurate rates for these processes requires numerical simulations of planetesimal accretion, we now consider simulations of planet formation in the Kuiper belt.

3. COAGULATION SIMULATIONS

3.1. Background

Safronov (1969) invented the current approach to planetesimal accretion calculations. In his particle-in-a-box method, planetesimals are a statistical ensemble of masses with distributions of orbital eccentricities and inclinations (*Greenberg et al.,* 1978; *Wetherill and Stewart,* 1989, 1993; *Spaute et al.,* 1991). This statistical approximation is essential: N-body codes cannot follow the $n \sim 10^9$–10^{12} 1-km planetesimals required to build Pluto-mass or Earth-mass planets. For large numbers of objects on fairly circular orbits (e.g., $n \gtrsim 10^4$, $r \lesssim 1000$ km, and $e \lesssim 0.1$), the method is also accurate. With a suitable prescription for collision outcomes, solutions to the coagulation equation in the kinetic theory yield the evolution of n(m) with arbitrarily small errors (e.g., *Wetherill,* 1990; *Lee,* 2000; *Malyshkin and Goodman,* 2001).

In addition to modeling planet growth, the statistical approach provides a method for deriving the evolution of orbital elements for large ensembles of planetesimals. If we (1) assume the distributions of e and i for planetesimals follow a Rayleigh distribution and (2) treat their motions as perturbations of a circular orbit, we can use the Fokker-Planck equation to solve for small changes in the orbits due to gas drag, gravitational interactions, and physical colli-

sions (*Hornung et al.,* 1985; *Wetherill and Stewart,* 1993; *Ohtsuki et al.,* 2002). Although the Fokker-Planck equation cannot derive accurate orbital parameters for planetesimals and oligarchs near massive planets, it yields accurate solutions for the ensemble average e and i when orbital resonances and other dynamical interactions are not important (e.g., *Wetherill and Stewart,* 1993; *Weidenschilling et al.,* 1997; *Ohtsuki et al.,* 2002).

Several groups have implemented *Safronov*'s (1969) method for calculations relevant to the outer solar system (*Greenberg et al.,* 1984; *Stern,* 1995, 2005; *Stern and Colwell,* 1997a,b; *Davis and Farinella,* 1997; *Kenyon and Luu,* 1998, 1999a,b; *Davis et al.,* 1999; *Kenyon and Bromley,* 2004a,d, 2005). These calculations adopt a disk geometry and divide the disk into N concentric annuli with radial width Δa_i at distances a_i from the central star. Each annulus is seeded with a set of planetesimals with masses m_{ij}, eccentricities e_{ij}, and inclinations i_{ij}, where the index i refers to one of N annuli and the index j refers to one of M mass batches within an annulus. The mass batches have mass spacing $\delta \equiv m_{j+1}/m_j$. In most calculations, $\delta \approx 2$; $\delta \leq 1.4$ is optimal (*Ohtsuki et al.,* 1990; *Wetherill and Stewart,* 1993; *Kenyon and Luu,* 1998).

Once the geometry is set, the calculations solve a set of coupled difference equations to derive the number of objects n_{ij} and the orbital parameters e_{ij} and i_{ij} as functions of time. Most studies allow fragmentation and velocity evolution through gas drag, collisional damping, dynamical friction, and viscous stirring. Because Q_D^* sets the maximum size $m_{c,max}$ of objects that participate in the collisional cascade, the size distribution for objects with $m < m_{c,max}$ depends on the fragmentation parameters (equation (8)) (*Davis and Farinella,* 1997; *Kenyon and Bromley,* 2004d; *Pan and Sari,* 2005). The size and velocity distributions of the merger population with $m > m_{c,max}$ are established during runaway growth and the early stages of oligarchic growth. Accurate treatment of velocity evolution is important for following runaway growth and thus deriving good estimates for the growth times and the size and velocity distributions of oligarchs.

When a few oligarchs contain most of the mass, collision rates depend on the orbital dynamics of individual objects instead of ensemble averages. *Safronov*'s (1969) statistical approach then fails (e.g., *Wetherill and Stewart,* 1993; *Weidenschilling et al.,* 1997). Although N-body methods can treat the evolution of the oligarchs, they cannot follow the evolution of leftover planetesimals, where the statistical approach remains valid (e.g., *Weidenschilling et al.,* 1997). *Spaute et al.* (1991) solve this problem by adding a Monte Carlo treatment of binary interactions between large objects to their multiannulus coagulation code. *Bromley and Kenyon* (2006) describe a hybrid code, which merges a direct N-body code with a multiannulus coagulation code. Both codes have been applied to terrestrial planet formation, but not to the Kuiper belt.

Current calculations cannot follow collisional growth accurately in an entire planetary system. Although the 6 order of magnitude change in formation timescales from ~0.4 AU to 40 AU is a factor in this statement, most modern supercomputers cannot finish calculations involving the entire disk with the required spatial resolution on a reasonable timescale. For the Kuiper belt, it is possible to perform a suite of calculations in a disk extending from 30–150 AU following 1-m and larger planetesimals. These calculations yield robust results for the mass distribution as a function of space and time and provide interesting comparisons with observations. Although current calculations do not include complete dynamical interactions with the giant planets or passing stars (see, e.g., *Charnoz and Morbidelli,* 2007), sample calculations clearly show the importance of external perturbations in treating the collisional cascade. We begin with a discussion of self-stirring calculations without interactions with the giant planets or passing stars and then describe results with external perturbers.

3.2. Self-Stirring

To illustrate *in situ* KBO formation at 40–150 AU, we consider a multiannulus calculation with an initial ensemble of 1-m to 1-km planetesimals in a disk with $\Sigma_{0d} = 0.12$ g cm^{-2}. The planetesimals have initial radii of 1 m to 1 km (with equal mass per logarithmic bin), $e_0 = 10^{-4}$, $i_0 = e_0/2$, mass density $\rho = 1.5$ g cm^{-3}, and fragmentation parameters $Q_b = 10^3$ erg g^{-1}, $Q_g = 1.5$ erg cm^{-3}, $\beta_b = 0$, and $\beta_g = 1.25$ (dashed curve in Fig. 1) (*Kenyon and Bromley,* 2004d, 2005). [Our choice of mass density is a compromise between pure ice ($\rho = 1$ g cm^{-3}) and the measured density of Pluto ($\rho \approx 2$ g cm^{-3}) (*Null et al.,* 1993). The calculations are insensitive to factor of 2 variations in the mass density of planetesimals.] The gas density also follows a MMSN, with $\Sigma_g/\Sigma_d = 100$ and a vertical scale height $h = 0.1\ r^{9/8}$ (*Kenyon and Hartmann,* 1987). The gas density is $\Sigma_g \propto e^{-t/t_g}$, with $t_g = 10$ m.y.

This calculation uses an updated version of the *Bromley and Kenyon* (2006) code that includes a Richardson extrapolation procedure in the coagulation algorithm. As in the Eulerian (*Kenyon and Luu,* 1998) and fourth-order Runge-Kutta (*Kenyon and Bromley,* 2002a,b) methods employed previously, this code provides robust numerical solutions to kernels with analytic solutions (e.g., *Ohtsuki et al.,* 1990; *Wetherill,* 1990) without producing the wavy size distributions described in other simulations with a low-mass cutoff (e.g., *Campo Bagatin et al.,* 1994). Once the evolution of large ($r > 1$ m) objects is complete, a separate code tracks the evolution of lower-mass objects and derives the dust emission as a function of time.

Figure 2 shows the evolution of the mass and eccentricity distributions at 40–47 AU for this calculation. During the first few million years, the largest objects grow slowly. Dynamical friction damps the orbits of the largest objects; collisional damping and gas drag circularize the orbits of the smallest objects. This evolution erases many of the initial conditions and enhances gravitational focusing by factors of 10–1000. Runaway growth begins. A few (and some-

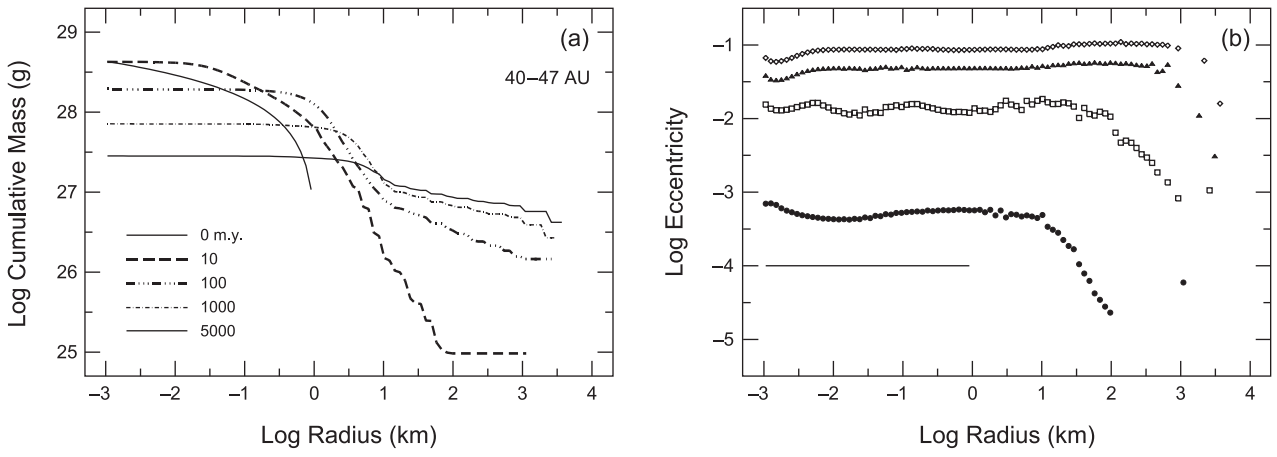

Fig. 2. Evolution of a multiannulus coagulation model with $\Sigma = 0.12(a_i/40\ \mathrm{AU})^{-3/2}$ g cm^{-2}. **(a)** Cumulative mass distribution at times indicated in the legend. **(b)** Eccentricity distributions at t = 0 (light solid line), t = 10 m.y. (filled circles), t = 100 m.y. (open boxes), t = 1 G.y. (filled triangles), and t = 5 G.y. (open diamonds). As large objects grow in the disk, they stir up the leftover planetesimals to e ~ 0.1. Disruptive collisions then deplete the population of 0.1–10-km planetesimals, which limits the growth of the largest objects.

times only one) oligarchs then grow from r ~ 10 km to r ~ 1000 km in ~30 m.y. at 40 AU and in ~1 G.y. at 150 AU (see equation (5)). Throughout runaway growth, dynamical friction and viscous stirring raise the random velocities of the leftover planetesimals to e ≈ 0.01–0.1 and i ≈ 2°–4° (v ~ 50–500 m s^{-1} at 40–47 AU; Fig. 2b). Stirring reduces gravitational focusing factors and ends runaway growth. The large oligarchs then grow slowly through accretion of leftover planetesimals.

As oligarchs grow, collisions among planetesimals initiate the collisional cascade. Disruptive collisions dramatically reduce the population of 1–10-km objects, which slows the growth of oligarchs and produces a significant debris tail in the size distribution. In these calculations, disruptive collisions remove material from the disk faster than oligarchs can accrete the debris. Thus, growth stalls and produces ~10–100 objects with maximum sizes r_{max} ~ 1000–3000 km at 40–50 AU (*Stern and Colwell,* 1997a,b; *Kenyon and Bromley,* 2004d, 2005; *Stern,* 2005).

Stochastic events lead to large dispersions in the growth time for oligarchs, t_o (equation (5)). In ensembles of 25–50 simulations with identical starting conditions, an occasional oligarch will grow up to a factor of 2 faster than its neighbors. This result occurs in simulations with δ = 1.4, 1.7, and 2.0, and thus seems independent of mass resolution. These events occur in ~25% of the simulations and lead to factor of ~2 variations in t_0 (equation (5)).

In addition to modest-sized icy planets, oligarchic growth generates copious amounts of dust (Fig. 3). When runaway growth begins, collisions produce small amounts of dust from "cratering" (see, e.g., *Greenberg et al.,* 1978; *Wetherill and Stewart,* 1993; *Stern and Colwell,* 1997a,b; *Kenyon and Luu,* 1999a). Stirring by growing oligarchs leads to "catastrophic" collisions, where colliding planetesimals lose more than 50% of their initial mass. These disruptive collisions produce a spike in the dust production rate that coincides with the formation of oligarchs with r ≥ 200–300 km (equation (9)). As the wave of runaway growth propagates outward, stirring produces disruptive collisions at ever-larger heliocentric distances. The dust mass grows in time and peaks at ~1 G.y., when oligarchs reach their maximum mass at 150 AU. As the mass in leftover planetesimals de-

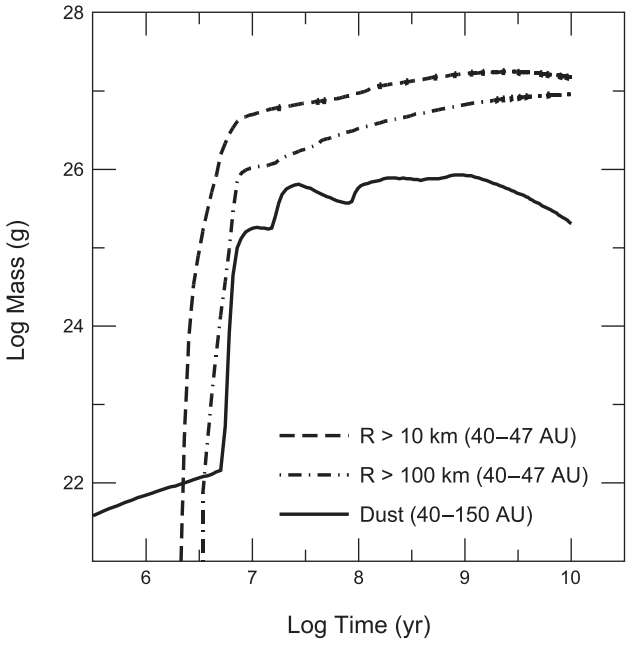

Fig. 3. Time evolution of the mass in KBOs and dust grains. Solid line: dust mass (r ≤ 1 mm) at 40–150 AU. Dashed (dot-dashed) lines: total mass in small (large) KBOs at 40–47 AU.

clines, Poynting-Robertson drag removes dust faster than disruptive collisions produce it. The dust mass then declines with time.

3.3. External Perturbation

Despite the efficiency of self-stirring models in removing leftover planetesimals from the disk, other mechanisms must reduce the derived mass in KBOs to current observational limits. In self-stirring calculations at 40–50 AU, the typical mass in KBOs with r ~ 30–1000 km at 4–5 G.y. is a factor of 5–10 larger than currently observed (*Luu and Jewitt,* 2002; chapter by Petit et al.). Unless Earth-mass or larger objects form in the Kuiper belt (*Chiang et al.,* 2007; *Levison and Morbidelli,* 2007), external perturbations must excite KBO orbits and enhance the collisional cascade.

Two plausible sources of external perturbation can reduce the predicted KBO mass to the desired limits. Once Neptune achieves its current mass and orbit, it stirs up the orbits of KBOs at 35–50 AU (*Levison and Duncan,* 1990; *Holman and Wisdom,* 1993; *Duncan et al.,* 1995; *Kuchner et al.,* 2002; *Morbidelli et al.,* 2004). In ~100 m.y. or less, Neptune removes nearly all KBOs with a ≤ 37–38 AU. Beyond a ~ 38 AU, some KBOs are trapped in orbital resonance with Neptune (*Malhotra,* 1995, 1996); others are ejected into the scattered disk (*Duncan and Levison,* 1997). In addition to these processes, Neptune stirring increases the effectiveness of the collisional cascade (*Kenyon and Bromley,* 2004d), which removes additional mass from the population of 0.1–10-km KBOs and prevents growth of larger KBOs.

Passing stars can also excite KBO orbits and enhance the collisional cascade. Although Neptune dynamically ejects scattered disk objects with perihelia q ≲ 36–37 AU (*Morbidelli et al.,* 2004), objects with q ≳ 45–50 AU, such as Sedna and Eris, require another scattering source. Without evidence for massive planets at a ≳ 50 AU (*Morbidelli et al.,* 2002), a passing star is the most likely source of the large q for these KBOs (*Morbidelli and Levison,* 2004; *Kenyon and Bromley,* 2004c).

Adams and Laughlin (2001) (see also chapter by Duncan et al.) examined the probability of encounters between the young Sun and other stars. Most stars form in dense clusters with estimated lifetimes of ~100 m.y. To account for the abundance anomalies of radionuclides in solar system meteorites (produced by supernovae in the cluster) and for the stability of Neptune's orbit at 30 AU, the most likely solar birth cluster has ~2000–4000 members, a crossing time of ~1 m.y., and a relaxation time of ~10 m.y. The probability of a close encounter with a distance of closest approach a_{close} is then ~60% $(a_{close}/160\ AU)^2$ (*Kenyon and Bromley,* 2004c).

Because the dynamical interactions between KBOs in a coagulation calculation and large objects like Neptune or a passing star are complex, here we consider simple calculations of each process. To illustrate the evolution of KBOs after a stellar flyby, we consider a very close pass with a_{close} = 160 AU (*Kenyon and Bromley,* 2004c). This corotating flyby produces objects with orbital parameters similar to those of Sedna and Eris. For objects in the coagulation calculation, the flyby produces an e distribution

$$e_{KBO} = \begin{cases} 0.025(a/30\ AU)^4 & a < a_0 \\ 0.5 & a > a_0 \end{cases} \qquad (10)$$

with $a_0 \approx 65$ AU (see *Ida et al.,* 2000; *Kenyon and Bromley,* 2004c; *Kobayashi et al.,* 2005). This e distribution produces a dramatic increase in the debris production rate throughout the disk, which freezes the mass distribution of the largest objects. (The i distribution following a flyby depends on the relative orientations of two planes, the orbital plane of KBOs and the plane of the trajectory of the passing star. Here, we assume the flyby produces no change in i, which simplifies the discussion without changing any of the results significantly.) Thus, to produce an ensemble of KBOs with r ≳ 300 km at 40–50 AU, the flyby must occur when the Sun has an age $t_\odot \gtrsim$ 10–20 m.y. (Fig. 2). For $t_\odot \gtrsim$ 100 m.y., the flyby is very unlikely. As a compromise between these two estimates, we consider a flyby at $t_\odot$ ~ 50 m.y.

Figure 4 shows the evolution of the KBO surface density in three annuli as a function of time. At early times (t ≲ 50 m.y.), KBOs grow in the standard way. After the flyby, the disk suffers a dramatic loss of material. At 40–47 AU, the disk loses ~90% (93%) of its initial mass in ~1 G.y. (4.5 G.y.). At ~50–80 AU, the collisional cascade removes ~90% (97%) of the initial mass in ~500 m.y. (4.5 G.y.). Beyond ~80 AU, KBOs contain less than 1% of the initial mass. Compared to self-stirring models, flybys that produce Sedna-like orbits are a factor of 2–3 more efficient at removing KBOs from the solar system.

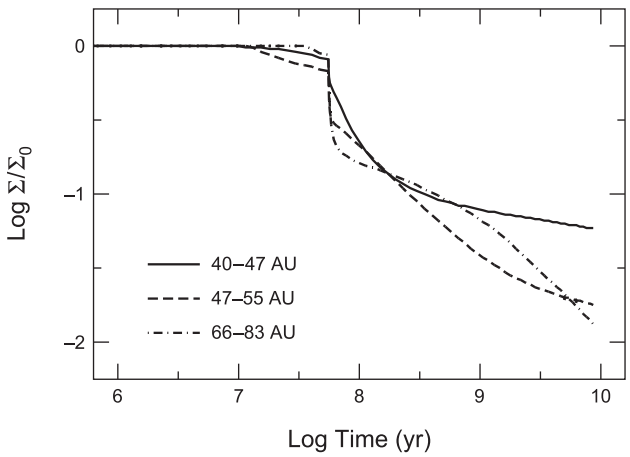

Fig. 4. Evolution of Σ after a stellar flyby. After 50 m.y. of growth, the close pass excites KBOs to large e (equation (10)) and enhances the collisional cascade.

To investigate the impact of Neptune on the collisional cascade, we parameterize the growth of Neptune at 30 AU as a simple function of time (*Kenyon and Bromley,* 2004d)

$$M_{Nep} \approx \begin{cases} 6 \times 10^{27}\ e^{(t - t_N)/t_1}\ g & t < t_N \\ 6 \times 10^{27}\ g + C(t - t_1) & t_N < t < t_2 \\ 1.0335 \times 10^{29}\ g & t > t_2 \end{cases} \quad (11)$$

where $C_{Nep} = 1.927 \times 10^{21}$ g yr^{-1}, $t_N = 50$ m.y., $t_1 = 3$ m.y., and $t_2 = 100$ m.y. These choices enable a model Neptune to reach a mass of 1 $M_\oplus$ in 50 m.y., when the largest KBOs form at 40–50 AU, and reach its current mass in 100 m.y. (This prescription is not intended as an accurate portrayal of Neptune formation, but it provides a simple way to investigate how Neptune might stir the Kuiper belt once massive KBOs form.) As Neptune approaches its final mass, its gravity stirs up KBOs at 40–60 AU and increases their orbital eccentricities to e ~ 0.1–0.2 on short timescales. In the coagulation model, distant planets produce negligible changes in i, so self-stirring sets i in these calculations (*Weidenschilling,* 1989). This evolution enhances debris production by a factor of 3–4, which effectively freezes the mass distribution of 100–1000-km objects at 40–50 AU. By spreading the leftover planetesimals and the debris over a larger volume, Neptune stirring limits the growth of the oligarchs and thus reduces the total mass in KBOs.

Figure 5 shows the evolution of the surface density in small and large KBOs in two annuli as a function of time. At 40–55 AU, Neptune rapidly stirs up KBOs to e ~ 0.1 when it reaches its current mass at ~100 m.y. Large collision velocities produce more debris, which is rapidly ground to dust and removed from the system by radiation pressure at early times and by Poynting-Robertson drag at later times. Compared to self-stirring models, the change in Σ is dramatic, with only ~3% of the initial disk mass remaining at ~4.5 G.y.

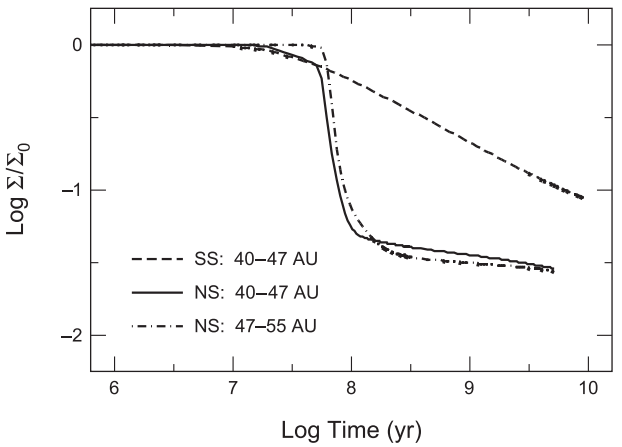

Fig. 5. Evolution of Σ (KBO) in models with Neptune stirring. Compared to self-stirring models (SS; dashed curve), stirring by Neptune rapidly removes KBOs at 40–47 AU (NS; solid curve) and at 47–55 AU (NS; dot-dashed curve).

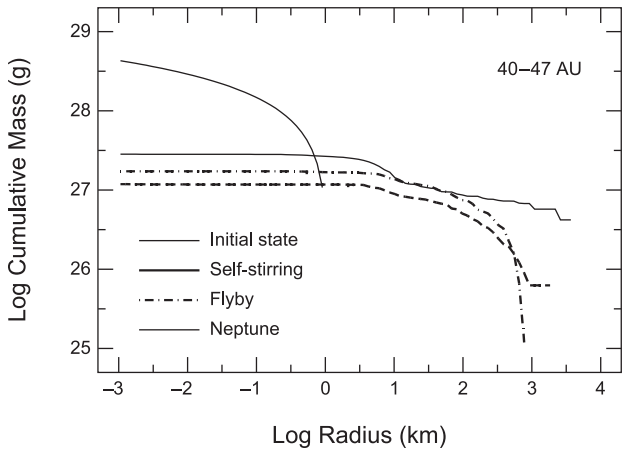

Fig. 6. Mass distributions for evolution with self-stirring (heavy solid line), stirring from a passing star (dot-dashed line), and stirring from Neptune at 30 AU (dashed line). After 4.5 G.y., the mass in KBOs with r ≥ 50 km is 5% (self-stirring), ~3.5% (flyby), and ~2% (Neptune stirring) of the initial mass. The number of objects with r ≥ 1000 km is ~100 (self-stirring), 1 (flyby), and 10 (Neptune stirring). The largest object has r_{max} ~ 3000 km (self-stirring), r_{max} ~ 500–1000 km (flyby), and r_{max} ~ 1000–2000 km (Neptune stirring).

From these initial calculations, it is clear that external perturbations dramatically reduce the mass of KBOs in the disk (see also *Charnoz and Morbidelli,* 2007). Figure 6 compares the mass distributions at 40–47 AU and at 4.5 G.y. for the self-stirring model in Fig. 2 (solid line) with results for the flyby (dot-dashed line) and Neptune stirring (dashed line). Compared to the self-stirring model, the close flyby reduces the mass in KBOs by ~50%. Neptune stirring reduces the KBO mass by almost a factor of 3 relative to the self-stirring model. For KBOs with r ≥ 30–50 km, the predicted mass in KBOs with Neptune stirring is within a factor of 2–3 of the current mass in KBOs.

These simple calculations for the stellar flyby and Neptune stirring do not include dynamical depletion. In the stellar flyby picture, the encounter removes nearly all KBOs beyond a truncation radius, $a_T \sim 48\ (a_{close}/160\ AU)$ AU (*Kenyon and Bromley,* 2004c). Thus, a close pass with a_{close} ~ 160 AU can produce the observed outer edge of the Kuiper belt at 48 AU. Although many objects with initial $a > a_T$ are ejected from the solar system, some are placed on very elliptical, Sedna-like orbits. [*Levison et al.* (2004) consider the impact of the flyby on the scattered disk and Oort cloud. After analyzing a suite of numerical simulations, they conclude that the flyby must occur before Neptune reaches its current orbit and begins the dynamical processes that populate the Oort cloud and the scattered disk. If Neptune forms *in situ* in 1–10 m.y., then the flyby cannot occur after massive KBOs form. If Neptune migrates to 30 AU after massive KBOs form, then a flyby can truncate the Kuiper belt without much impact on the Oort cloud or the scattered disk.] In the Neptune-stirring model, dynamical interactions will eject some KBOs at 40–47 AU. If the dynamical in-

teractions that produce the scattered disk reduce the mass in KBOs by a factor of 2 at 40–47 AU (e.g., *Duncan et al.,* 1995; *Kuchner et al.,* 2002), the Neptune-stirring model yields a KBO mass in reasonably good agreement with observed limits (for a different opinion, see *Charnoz and Morbidelli,* 2007).

3.4. Nice Model

Although *in situ* KBO models can explain the current amount of mass in large KBOs, these calculations do not address the orbits of the dynamical classes of KBOs. To explain the orbital architecture of the giant planets, the "Nice group" centered at Nice Observatory developed an inspired, sophisticated picture of the dynamical evolution of the giant planets and a remnant planetesimal disk (*Tsiganis et al.,* 2005; *Morbidelli et al.,* 2005; *Gomes et al.,* 2005, and references therein). The system begins in an approximate equilibrium, with the giant planets in a compact configuration (Jupiter at 5.45 AU, Saturn at ~8.2 AU, Neptune at ~11.5 AU, and Uranus at ~14.2 AU) and a massive planetesimal disk at 15–30 AU. Dynamical interactions between the giant planets and the planetesimals lead to an instability when Saturn crosses the 2:1 orbital resonance with Jupiter, which results in a dramatic orbital migration of the gas giants and the dynamical ejection of planetesimals into the Kuiper belt, scattered disk, and the Oort cloud. Comparisons between the end state of this evolution and the orbits of KBOs in the "hot population" and the scattered disk are encouraging (chapter by Morbidelli et al.).

Current theory cannot completely address the likelihood of the initial state in the Nice model. *Thommes et al.* (1999, 2002) demonstrate that n-body simulations can produce a compact configuration of gas giants, but did not consider how fragmentation or interactions with low-mass planetesimals affect the end state. *O'Brien et al.* (2005) show that a disk of planetesimals has negligible collisional grinding over 600 m.y. if most of the mass is in large planetesimals with $r \gtrsim 100$ km. However, they did not address whether this state is realizable starting from an ensemble of 1-km and smaller planetesimals. In terrestrial planet simulations starting with 1–10-km planetesimals, the collisional cascade removes ~25% of the initial rocky material in the disk (*Wetherill and Stewart,* 1993; *Kenyon and Bromley,* 2004b). Interactions between oligarchs and remnant planetesimals are also important for setting the final mass and dynamical state of the terrestrial planets (*Bromley and Kenyon,* 2006; *Kenyon and Bromley,* 2006). Because complete hybrid calculations of the giant planet region are currently computationally prohibitive, it is not possible to make a reliable assessment of these issues for the formation of gas giant planets.

Here, we consider the evolution of the planetesimal disk outside the compact configuration of giant planets, where standard coagulation calculations can follow the evolution of many initial states for 1–5 G.y. in a reasonable amount of computer time. Figure 7 shows the time evolution for the surface density of planetesimals in three annuli from one typical calculation at 20–25 AU (dot-dashed curve; M_i = 6 $M_\oplus$), 36–44 AU (dashed curve; M_i = 9 $M_\oplus$), and 66–83 AU (solid curve; M_i = 12 $M_\oplus$). Starting from the standard surface density profile (equation (1)), planetesimals at 20–25 AU grow to 1000-km sizes in a few million years. Once the collisional cascade begins, the surface density slowly declines to ~10% to 20% of its initial value at the time of the late heavy bombardment, when the Nice model predicts that Saturn crosses the 2:1 orbital resonance with Jupiter.

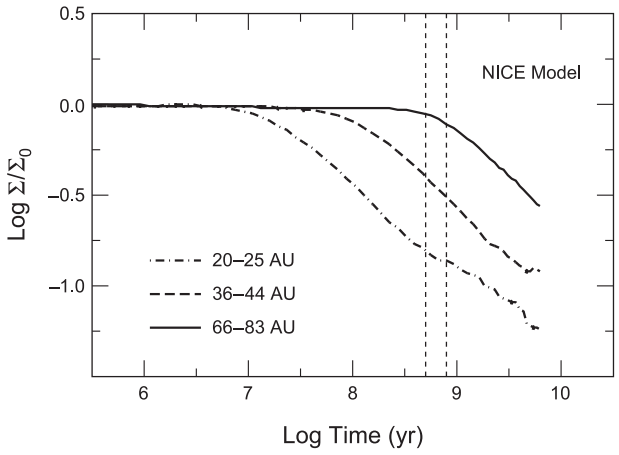

Fig. 7. Evolution of Σ in a self-stirring model at 20–100 AU. At 20–25 AU, it takes 5–10 m.y. to form 1000-km objects. After ~0.5–1 G.y., there are ~100 objects with r ~ 1000–2000 km and ~10^5 objects with r ~ 100–200 km at 20–30 AU. As these objects grow, the collisional cascade removes 90% of the mass in remnant planetesimals. The twin vertical dashed lines bracket the time of the late heavy bombardment at 300–600 m.y.

These results provide a strong motivation to couple coagulation calculations with the dynamical simulations of the Nice group (see also *Charnoz and Morbidelli,* 2007). In the Nice model, dynamical interactions with a massive planetesimal disk are the "fuel" for the dramatic migration of the giant planets and the dynamical ejection of material into the Kuiper belt and the scattered disk. If the mass in the planetesimal disk declines by ~80% as the orbits of the giant planets evolve, the giant planets cannot migrate as dramatically as in the *Gomes et al.* (2005) calculations. Increasing the initial mass in the disk by a factor of 3–10 may allow coagulation and the collisional cascade to produce a debris disk capable of triggering the scattering events of the Nice model.

3.5. A Caveat on the Collisional Cascade

Although many of the basic outcomes of oligarchic growth and the collisional cascade are insensitive to the initial conditions and fragmentation parameters for the planetesimals, several uncertainties in the collisional cascade can modify the final mass in oligarchs and the distributions of r and e. Because current computers do not allow coagulation calculations that include the full range of sizes (1 μm

to 10^4 km), published calculations have two pieces, a solution for large objects (e.g., *Kenyon and Bromley,* 2004a,b) and a separate solution for smaller objects (e.g., *Krivov et al.,* 2006). Joining these solutions assumes that (1) collision fragments continue to collide and fragment until particles are removed by radiative processes and (2) mutual (destructive) collisions among the fragments are more likely than mergers with much larger oligarchs. These assumptions are reasonable but untested by numerical calculations (*Kenyon and Bromley,* 2002a). Thus, it may be possible to halt or to slow the collisional cascade before radiation pressure rapidly removes small grains with $r \approx 1$–100 μm.

In current coagulation calculations, forming massive oligarchs at 5–15 AU in a massive disk requires an inefficient collisional cascade. When the cascade is efficient, the most massive oligarchs have $m \lesssim M_\oplus$. Slowing the cascade allows oligarchs to accrete planetesimals more efficiently, which results in larger oligarchs that contain a larger fraction of the initial mass. If collisional damping is efficient, halting the cascade completely at sizes of ~1 mm leads to rapid *in situ* formation of Uranus and Neptune (*Goldreich et al.,* 2004) and early stirring of KBOs at 40 AU.

There are two simple ways to slow the collisional cascade. In simulations where the cascade continues to small sizes, $r \sim 1$–10 μm, the radial optical depth in small grains is $\tau_s \sim 0.1$–1 at 30–50 AU (*Kenyon and Bromley,* 2004a). Lines-of-sight to the central star are not purely radial, so this optical depth reduces radiation pressure and Poynting-Robertson drag by small factors, $\sim e^{-0.2\tau_s} \sim 10$–$30\%$, and has little impact on the evolution of the cascade. With $\tau_s \propto a^{-s}$ and $s \sim 1$–2, however, the optical depth may reduce radiation forces significantly at smaller a. Slowing the collisional cascade by factors of 2–3 could allow oligarchs to accrete leftover planetesimals and smaller objects before the cascade removes them.

Collisional damping and gas drag on small particles may also slow the collisional cascade. For particles with large ratios of surface area to volume, $r \lesssim 0.1$–10 cm, collisions and the gas effectively damp e and i (*Adachi et al.,* 1976; *Goldreich et al.,* 2004) and roughly balance dynamical friction and viscous stirring. Other interactions between small particles and the gas — such as photophoresis (*Wurm and Krauss,* 2006) — also damp particles random velocities and thus might help to slow the cascade. Both collisions and interactions between the gas and the solids are more effective at large volume density, so these processes should be more important inside 30 AU than outside 30 AU. The relatively short lifetime of the gas, ~3–10 m.y., also favors more rapid growth inside 30 AU. If damping maintains an equilibrium $e \sim 10^{-3}$ at $a \sim 20$–30 AU, oligarchs can grow to the sizes required in the Nice model ($r \gtrsim 2000$ km). Rapid growth at $a \sim 5$–15 AU might produce oligarchs with the isolation mass ($r \sim 10$–$30\ R_\oplus$; equation (6)) and lead to the rapid formation of gas giants.

Testing these mechanisms for slowing the collisional cascade requires coagulation calculations with accurate treatments of collisional damping, gas drag, and optical depth for particle radii $r \sim 1$–10 μm to $r \sim 10{,}000$ km. Although these calculations require factors of 4–6 more computer time than published calculations, they are possible with multiannulus coagulation codes on modern parallel computers.

3.6. Model Predictions

The main predictions derived from coagulation models are n(r), n(e), and n(i) as functions of a. The cumulative number distribution consists of three power laws (*Kenyon and Bromley,* 2004d; *Pan and Sari,* 2005)

$$n(r) = \begin{cases} n_d r^{-\alpha_d} & r \le r_1 \\ n_1 & r_1 \le r \le r_0 \\ n_m r^{-\alpha_m} & r \ge r_0 \end{cases} \qquad (12)$$

The debris population at small sizes, $r \le r_1$, always has $\alpha_d \approx 3.5$. The merger population at large sizes, $r \ge r_0$, has $\alpha_m \approx 2.7$–4. Because the collisional cascade robs oligarchs of material, calculations with more stirring have steeper size distributions. Thus, self-stirring calculations with $Q_b \ge 10^5$ erg g^{-1} ($Q_b \lesssim 10^3$ erg g^{-1}) typically yield $\alpha_m \approx 2.7$–3.3 (3.5–4). Models with a stellar flyby or stirring by a nearby gas giant also favor large α_m.

The transition radii for the power laws depend on the fragmentation parameters (see Fig. 1) (see also *Pan and Sari,* 2005). For a typical $e \sim 0.01$–0.1 in self-stirring models, $r_0 \approx r_1 \approx 1$ km when $Q_b \ge 10^5$ erg g^{-1}. When $Q_b \lesssim 10^3$ erg g^{-1}, $r_1 \approx 0.1$ km and $r_0 \approx 10$–20 km. Thus the calculations predict a robust correlation between the transition radii and the power law exponents: large r_0 and α_m or small r_0 and α_m.

Because gravitational stirring rates are larger than accretion rates, the predicted distributions of e and i at 4–5 G.y. depend solely on the total mass in oligarchs (see also *Goldreich et al.,* 2004). Small objects with $r \le r_0$ contain a very small fraction of the mass and cannot stir themselves. Thus e and i are independent of r (Fig. 2). The e and i for larger objects depends on the total mass in the largest objects. In self-stirring models, dynamical friction and viscous stirring between oligarchs and planetesimals (during runaway growth) and among the ensemble of oligarchs (during oligarchic growth) set the distribution of e for large objects with $r \ge r_0$. In self-stirring models, viscous stirring among oligarchs dominates dynamical friction between oligarchs and leftover planetesimals, which leads to a shallow relation between e and r, $e \propto r^{-\gamma}$ with $\gamma \approx 3/4$. In the flyby and Neptune-stirring models, stirring by the external perturber dominates stirring among oligarchs. This stirring yields a very shallow relation between e and r with $\gamma \approx 0$–0.25.

Other results depend little on the initial conditions and the fragmentation parameters. In calculations with different initial mass distributions, an order of magnitude range in e_0, and $Q_b = 10^0$–10^7 erg g^{-1}, $\beta_b = 0.5$–0, $Q_g = 0.5$–5 erg cm^{-3}, $\beta_b \ge 1.25$, r_{max} and the amount of mass removed by

the collisional cascade vary by ≤10% relative to the evolution of the models shown in Figs. 2–7. Because collisional damping among 1-m to 1-km objects erases the initial orbital distribution, the results do not depend on e_0 and i_0. Damping and dynamical friction also quickly erase the initial mass distribution, which yields growth rates that are insensitive to the initial mass distribution.

The insensitivity of r_{max} and mass removal to the fragmentation parameters depends on the rate of collisional disruption relative to the growth rate of oligarchs. Because the collisional cascade starts when $m_o \sim m_d$ (equation (9)), calculations with small Q_b ($Q_b \leq 10^3$ erg g^{-1}) produce large amounts of debris before calculations with large Q_b ($Q_b \geq 10^3$ erg g^{-1}). Thus, an effective collisional cascade should yield lower mass oligarchs and more mass removal when Q_b is small. However, oligarchs with $m_o > m_d$ still have fairly large gravitational focusing factors and accrete leftover planetesimals more rapidly than the cascade removes them. As oligarchic growth continues, gravitational focusing factors fall and collision disruptions increase. All calculations then reach a point where the collisional cascade removes leftover planetesimals more rapidly than oligarchs can accrete them. As long as most planetesimals have r ~ 1–10 km, the timing of this epoch is more sensitive to gravitational focusing and the growth of oligarchs than the collisional cascade and the fragmentation parameters. Thus, r_{max} and the amount of mass processed through the collisional cascade are relatively insensitive to the fragmentation parameters.

4. CONFRONTING KUIPER BELT OBJECT COLLISION MODELS WITH KUIPER BELT OBJECT DATA

Current data for KBOs provide two broad tests of coagulation calculations. In each dynamical class, four measured parameters test the general results of coagulation models and provide ways to discriminate among the outcomes of self-stirring and perturbed models. These parameters are r_{max}, the size of the largest object; $\alpha_{m,}$ the slope of the size distribution for large KBOs with r ≥ 10 km; r_0, the break radius, which measures the radius where the size distribution makes the transition from a merger population ($r \geq r_0$) to a collisional population ($r \leq r_0$) as summarized in equation (12); and M_t, the total mass in large KBOs.

For all KBOs, measurements of the dust mass allow tests of the collisional cascade and link the Kuiper belt to observations of nearby debris disks. We begin with the discussion of large KBOs and then compare the Kuiper belt with other debris disks.

Table 1 summarizes the mass and size distribution parameters derived from recent surveys. To construct this table, we used online data from the Minor Planet Center (*cfa-www.harvard.edu/iau/lists/MPLists.html*) for r_{max} (see also *Levison and Stern,* 2001) and the results of several detailed analyses for α_m, r_{max}, and r_0 (e.g., *Bernstein et al.,* 2004; *Elliot et al.,* 2005; *Petit et al.,* 2006; chapter by Petit et al.).

TABLE 1. Data for KBO size distribution.

KBO Class	M_l ($M_\oplus$)	r_{max} (km)	r_0 (km)	q_m
Cold cl	0.01–0.05	400	20–40 km	≥4
Hot cl	0.01–0.05	1000	20–40 km	3–3.5
Detached	n/a	1500	n/a	n/a
Resonant	0.01–0.05	1000	20–40 km	3
Scattered	0.1–0.3	700	n/a	n/a

Because comprehensive KBO surveys are challenging, the entries in the table are incomplete and sometimes uncertain. Nevertheless, these results provide some constraints on the calculations.

Current data provide clear evidence for physical differences among the dynamical classes. For classical KBOs with a = 42–48 AU and q > 37 AU, the cold population (i ≤ 4°) has a steep size distribution with $\alpha_m \approx 3.5$–4 and $r_{max} \sim$ 300–500 km. In contrast, the hot population (i ≥ 10°) has a shallow size distribution with $\alpha_m \approx 3$ and $r_{max} \sim 1000$ km (*Levison and Stern,* 2001). Both populations have relatively few objects with optical brightness $m_R \approx 27$–27.5, which implies $r_0 \sim$ 20–40 km for reasonable albedo ~0.04–0.07. The detached, resonant, and scattered disk populations contain large objects with $r_{max} \sim 1000$ km. Although there are too few detached or scattered disk objects to constrain α_m or r_0, data for the resonant population are consistent with constraints derived for the hot classical population, $\alpha_m \approx 3$ and $r_0 \approx$ 20–40 km.

The total mass in KBOs is a small fraction of the ~10–30 $M_\oplus$ of solid material in a MMSN from ~35–50 AU (*Gladman et al.,* 2001; *Bernstein et al.,* 2004; *Petit et al.,* 2006; see also chapter by Petit et al.). The classical and resonant populations have $M_l \approx 0.01$–0.1 $M_\oplus$ in KBOs with r ≥ 10–20 km. The scattered disk may contain more material, $M_l \sim 0.3\ M_\oplus$, but the constraints are not as robust as for the classical and resonant KBOs.

These data are broadly inconsistent with the predictions of self-stirring calculations with no external perturbers. Although self-stirring models yield inclinations, i ≈ 2°–4°, close to those observed in the cold, classical population, the small r_{max} and the large α_m of this group suggest that an external dynamical perturbation — such as a stellar flyby or stirring by Neptune — modified the evolution once r_{max} reached ~300–500 km. The observed break radius, $r_0 \sim$ 20–40 km, also agrees better with the $r_0 \sim 10$ km expected from Neptune-stirring calculations than the 1 km achieved in self-stirring models (*Kenyon and Bromley,* 2004d; *Pan and Sari,* 2005). Although a large r_{max} and a small α_m for the resonant and hot, classical populations agree reasonably well with self-stirring models, the observed $r_{max} \sim 1000$ km is much smaller than the $r_{max} \sim$ 2000–3000 km typically achieved in self-stirring calculations (Fig. 1). Both of these populations appear to have large r_0, which is also more consistent with Neptune-stirring models than with self-stirring models.

The small M_l for all populations provides additional evidence against self-stirring models. In the most optimistic

scenario, where KBOs are easily broken, self-stirring models leave a factor of 5–10 more mass in large KBOs than currently observed at 40–48 AU. Although models with Neptune stirring leave a factor of 2–3 more mass in KBOs at 40–48 AU than is currently observed, Neptune ejects half the KBOs at 40–48 AU into the scattered disk (e.g., *Duncan et al.,* 1995; *Kuchner et al.,* 2002). With an estimated mass of 2–3× the mass in classical and resonant KBOs, the scattered disk contains enough material to bridge the difference between the KBO mass derived from Neptune-stirring models and the observed KBO mass.

The mass in KBO dust grains provides a final piece of evidence against self-stirring models. From an analysis of data from Pioneer 10 and 11, *Landgraf et al.* (2002) estimate a dust production rate of 10^{15} g yr^{-1} in 0.01–2-mm particles at 40–50 AU. The timescale for Poynting-Robertson drag to remove these grains from the Kuiper belt is ~10–100 m.y. (*Burns et al.,* 1979), which yields a mass of ~10^{22}–10^{24} g. Figure 8 compares this dust mass with masses derived from mid-IR and submillimeter observations of several nearby solar-type stars (*Greaves et al.,* 1998, 2004; *Williams et al.,* 2004; *Wyatt et al.,* 2005) and with predictions from the self-stirring, flyby, and Neptune-stirring models. The dust masses for nearby solar-type stars roughly follow the predictions of self-stirring models and flyby models with $Q_b \sim 10^3$ erg g^{-1}. The mass of dust in the Kuiper belt is 1–3 orders of magnitude smaller than predicted in self-stirring models and is closer to the predictions of the Neptune-stirring models.

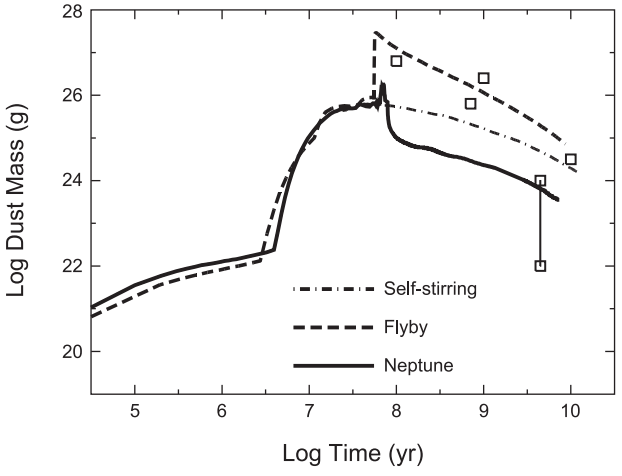

Fig. 8. Evolution of mass in small dust grains (0.001–1 mm) for models with self-stirring (dot-dashed line), stirring from a passing star (dashed line), and stirring from Neptune at 30 AU (solid line) for $Q_b = 10^3$ erg g^{-1}. Calculations with smaller (large) Q_b produce more (less) dust at $t \lesssim 50$ m.y. and somewhat more (less) dust at $t \gtrsim 100$ m.y. At 1–5 G.y., models with Neptune stirring have less dust than self-stirring or flyby models. The boxes show dust mass estimated for four nearby solar-type stars (from left to right in age: HD 107146, ε Eri, η Crv, and τ Cet) (*Greaves et al.,* 1998, 2004; *Williams et al.,* 2004; *Wyatt et al.,* 2005) and two estimates for the Kuiper belt (boxes connected by solid line) (*Landgraf et al.,* 2002).

To combine the dynamical properties of KBOs with these constraints, we rely on results from N-body simulations that do not include collisional processing of small objects (see chapter by Morbidelli et al.). For simplicity, we consider coagulation in the context of the Nice model, which provides a solid framework for interpreting the dynamics of the gas giants and the dynamical classes of KBOs. In the Nice model, Saturn's crossing of the 2:1 resonance with Jupiter initiates the dynamical instability that populates the Kuiper belt. As Neptune approaches $a \approx 30$ AU, it captures resonant KBOs, ejects KBOs into the scattered disk and the Oort cloud, and excites the hot classical KBOs. Although Neptune might reduce the number of cold, classical KBOs formed roughly *in situ* beyond 30 AU, the properties of these KBOs probably reflect conditions in the Kuiper belt when the instability began.

The Nice model requires several results from coagulation calculations. Once giant planets form at 5–15 AU, collisional growth must produce thousands of Pluto-mass objects at 20–30 AU. Unless the planetesimal disk was massive, growth of oligarchs must dominate collisional grinding in this region of the disk. To produce the cold classical population at ~45 AU, collisions must produce 1–10 Pluto-mass objects and then efficiently remove leftover planetesimals. To match the data in Table 1, KBOs formed at 20–30 AU should have a shallower size distribution and a larger r_{max} than those at 40–50 AU.

Some coagulation results are consistent with the trends required in the Nice model. In current calculations, collisional growth naturally yields smaller r_{max} and a steeper size distribution at larger a. At 40–50 AU, Neptune-stirring models produce a few Pluto-mass objects and many smaller KBOs with $e \sim 0.1$ and $i \approx 2°$–$4°$. Although collisional growth produces more Plutos at 15–30 AU than at 40–50 AU, collisional erosion removes material faster from the inner disk than from the outer disk (Fig. 7). Thus, collisions do not produce the thousands of Pluto-mass objects at 15–30 AU required in the Nice model.

Reconciling this aspect of the Nice model with the coagulation calculations requires a better understanding of the physical processes that can slow or halt the collisional cascade. Producing gas giants at 5–15 AU, thousands of Plutos at 20–30 AU, and a few or no Plutos at 40–50 AU implies that the outcome of coagulation changes markedly from 5 AU to 50 AU. If the collisional cascade can be halted as outlined in section 3.5, forming 5–10 $M_\oplus$ cores at 5–15 AU is straightforward. Slowing the collisional cascade at 20–30 AU might yield a large population of Pluto mass objects at 20–30 AU. Because α_m and r_{max} are well-correlated, better constraints on the KBO size distributions coupled with more robust coagulation calculations can test these aspects of the Nice model in more detail.

To conclude this section, we consider constraints on the Kuiper belt in the more traditional migration scenario of *Malhotra* (1995), where Neptune forms at ~20–25 AU and slowly migrates to 30 AU. To investigate the relative importance of collisional and dynamical depletion at 40–50 AU,

Charnoz and Morbidelli (2007) couple a collision code with a dynamical code and derive the expected distributions for size and orbital elements in the Kuiper belt, the scattered disk, and the Oort cloud. Although collisional depletion models can match the observations of KBOs, these models are challenged to provide enough small objects into the scattered disk and Oort cloud. Thus, the results suggest that dynamical mechanisms dominate collisions in removing material from the Kuiper belt.

Although *Charnoz and Morbidelli* (2007) argue against a dramatic change in collisional evolution from 15 AU to 40 AU, the current architecture of the solar system provides good evidence for this possibility. In the MMSN, the ratio of timescales to produce gas giant cores at 10 AU and at 25 AU is $\xi = (25/10)^3 \sim 15$. In the context of the Nice model, formation of Saturn and Neptune at 8–11 AU in 5–10 m.y. thus implies formation of other gas giant cores at 20–25 AU in 50–150 m.y. If these cores *had* formed, they would have consumed most of the icy planetesimals at 20–30 AU, leaving little material behind to populate the outer solar system when the giant planets migrate. The apparent lack of gas giant core formation at 20–30 AU indicates that the collisional cascade changed dramatically from 5–15 AU (where gas giant planets formed) to 20–30 AU (where gas giant planets did not form). As outlined in section 3.5, understanding the interaction of small particles with the gas and the radiation field may provide important insights into the evolution of oligarchic growth and thus into the formation and structure of the solar system.

5. KUIPER BELT OBJECTS AND ASTEROIDS

In many ways, the Kuiper belt is similar to the asteroid belt. Both are populations of small bodies containing relatively little mass compared to the rest of the solar system; the structure and dynamics of both populations have been influenced significantly by the giant planets; and both have been and continue to be significantly influenced by collisions. Due to its relative proximity to Earth, however, there are substantially more observational data available for the asteroid belt than the Kuiper belt. While the collisional and dynamical evolution of the asteroid belt is certainly not a solved problem, the abundance of constraints has allowed for the development of reasonably consistent models. Here we briefly describe what is currently understood about the evolution of the asteroid belt, what insights that may give us with regards to the evolution of the Kuiper belt, and what differences might exist in the evolution of the two populations.

It has long been recognized that the primordial asteroid belt must have contained hundreds or thousands of times more mass than the current asteroid belt (e.g., *Lecar and Franklin,* 1973; *Safronov,* 1979; *Weidenschilling,* 1977c; *Wetherill,* 1989). Reconstructing the initial mass distribution of the solar system from the current masses of the planets and asteroids, for example, yields a pronounced mass deficiency in the asteroid belt region relative to an otherwise smooth distribution for the rest of the solar system (*Weidenschilling,* 1977c). To accrete the asteroids on the timescales inferred from meteoritic evidence would require hundreds of times more mass than currently exists in the main belt (*Wetherill,* 1989).

In addition to its pronounced mass depletion, the asteroid belt is also strongly dynamically excited. The mean proper eccentricity and inclination of asteroids larger than ~50 km in diameter are 0.135 and 10.9° (from the catalog of *Knežević and Milani*, 2003), significantly larger than can be explained by gravitational perturbations among the asteroids or by simple gravitational perturbations from the planets (*Duncan,* 1994). The fact that the different taxonomic types of asteroids (S-type, C-type, etc.) are radially mixed somewhat throughout the main belt, rather than confined to delineated zones, indicates that there has been significant scattering in semimajor axis as well (*Gradie and Tedesco,* 1982).

Originally, a collisional origin was suggested for the mass depletion in the asteroid belt (*Chapman and Davis,* 1975). The difficulty of collisionally disrupting the largest asteroids, coupled with the survival of the basaltic crust of the ~500-km-diameter asteroid Vesta, however, suggest that collisional grinding was not the cause of the mass depletion (*Davis et al.,* 1979, 1985, 1989, 1994; *Wetherill,* 1989; *Durda and Dermott,* 1997; *Durda et al.,* 1998; *Bottke et al.,* 2005a,b; *O'Brien and Greenberg,* 2005). In addition, collisional processes alone could not fully explain both the dynamical excitation and the radial mixing observed in the asteroid belt, although *Charnoz et al.* (2001) suggest that collisional diffusion may have contributed to its radial mixing.

Several dynamical mechanisms have been proposed to explain the mass depletion, dynamical excitation, and radial mixing of the asteroid belt. As the solar nebula dissipated, the changing gravitational potential acting on Jupiter, Saturn, and the asteroids would lead to changes in their precession rates and hence changes in the positions of secular resonances, which could "sweep" through the asteroid belt, exciting e and i, and coupled with gas drag, could lead to semimajor axis mobility and the removal of material from the belt (e.g., *Heppenheimer,* 1980; *Ward,* 1981; *Lemaitre and Dubru,* 1991; *Lecar and Franklin,* 1997; *Nagasawa et al.,* 2000, 2001, 2002). It has also been suggested that sweeping secular resonances could lead to orbital excitation in the Kuiper belt (*Nagasawa and Ida,* 2000). However, as reviewed by *Petit et al.* (2002) and *O'Brien et al.* (2007), secular resonance sweeping is generally unable to simultaneously match the observed e and i excitation in the asteroid belt, as well as its radial mixing and mass depletion, for reasonable parameter choices (especially in the context of the Nice model).

Another possibility is that planetary embryos were able to accrete in the asteroid belt (e.g., *Wetherill,* 1992). The fact that Jupiter's ~10-$M_\oplus$ core was able to accrete in our solar system beyond the asteroid belt suggests that embryos were almost certainly able to accrete in the asteroid belt, even accounting for the roughly 3–4× decrease in the mass

density of solid material inside the snow line. The scattering of asteroids by those embryos, coupled with the jovian and saturnian resonances in the asteroid belt, has been shown to be able to reasonably reproduce the observed e and i excitation in the belt as well as its radial mixing and mass depletion (*Petit et al.,* 2001, 2002; *O'Brien et al.,* 2007). In the majority of simulations of this scenario by both groups, the embryos are completely cleared from the asteroid belt.

Thus, the observational evidence and theoretical models for the evolution of the asteroid belt strongly suggest that dynamics, rather than collisions, dominated its mass depletion. Collisions, however, have still played a key role in sculpting the asteroid belt. Many dynamical families, clusterings in orbital element space, have been discovered, giving evidence for ~20 breakups of 100-km or larger parent bodies over the history of the solar system (*Bottke et al.,* 2005a,b). The large 500-km-diameter asteroid Vesta has a preserved basaltic crust with a single large impact basin (*McCord et al.,* 1970; *Thomas et al.,* 1997). This basin was formed by the impact of a roughly 40-km projectile (*Marzari et al.,* 1996; *Asphaug,* 1997).

The size distribution of main-belt asteroids is known or reasonably constrained through observational surveys down to ~1 km in diameter (e.g., *Durda and Dermott,* 1997; *Jedicke and Metcalfe,* 1998; *Ivezić et al.,* 2001; *Yoshida et al.,* 2003; *Gladman et al.* 2007). Not surprisingly, the largest uncertainties are at the smallest sizes, where good orbits are often not available for the observed asteroids, which makes the conversion to absolute magnitude and diameter difficult (e.g., *Ivezić et al.,* 2001; *Yoshida et al.,* 2003). Recent results from the Sub-Kilometer Asteroid Diameter Survey (SKADS) (*Gladman et al.,* 2007), the first survey since the Palomar-Leiden Survey designed to determine orbits as well as magnitudes of main-belt asteroids, suggest that the asteroid magnitude-frequency distribution may be well represented by a single power law in the range from H = 14.0 to 18.8, which corresponds to diameters of 0.7 to 7 km for an albedo of 0.11. These observational constraints are shown in Fig. 9 alongside the determination of the TNO size distribution from *Bernstein et al.* (2004).

While over some size ranges, the asteroid size distribution can be fit by a single power law, over the full range of observed asteroid diameters from ~1–1000 km there are multiple bumps or kinks in the size distribution (namely around 10 and 100 km in diameter). The change in slope of the size distribution around 100 km is due primarily to the fact that asteroids larger than this are very difficult to disrupt, and hence the size distribution of bodies larger than 100 km is likely primordial. The change in slope around 10 km has a different origin — such a structure is produced as a result of a change in the strength properties of asteroids, namely the transition from when a body's resistance to disruption is dominated by material strength to when it is dominated by self-gravity. This transition in strength properties occurs at a size much smaller than 10 km, but results in a structure that propagates to larger sizes (see, e.g., *Durda et al.,* 1998; *O'Brien and Greenberg,* 2003). The presence of this structure in the asteroid size distribution is consistent with the asteroids being a collisionally relaxed population, i.e., a population in which the size distribution has reached an approximate steady state where collisional production and collisional destruction of bodies in each size range are in balance.

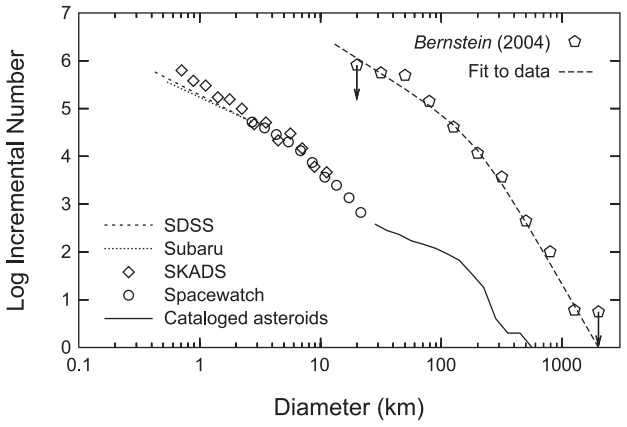

Fig. 9. Observational estimates of the main belt and TNO size distributions. The pentagons (with dashed best-fit curve) show the total TNO population as determined from the *Bernstein et al.* (2004) HST survey, converted to approximate diameters assuming an albedo of 0.04. Points with arrows are upper limits given by nondetections. The solid line is the population of observed asteroids, and open circles are from debiased Spacewatch main-belt observations (*Jedicke and Metcalfe,* 1998). These data, converted to diameters, were provided by D. Durda. The two dashed lines are extrapolations based on the Sloan Digital Sky Survey (*Ivezić et al.,* 2001) and the Subaru Subkilometer Main Belt Asteroid Survey (*Yoshida et al.,* 2003), and diamonds show the debiased population estimate from the SKADS survey (*Gladman et al.,* 2007). Error bars are left out of this plot for clarity. Note that the TNO population is substantially more populous and massive, by roughly a factor of 1000, than the asteroid population.

The collisional evolution of the asteroid belt has been studied by many authors (e.g., *Davis et al.,* 1985, 1994; *Durda,* 1993; *Durda and Dermott,* 1997; *Durda et al.,* 1998; *Campo Bagatin et al.,* 1993, 1994, 2001; *Marzari et al.,* 1999). The most recent models of collisional evolution of the asteroid belt incorporate aspects of dynamical evolution as well, such as the removal of bodies by resonances and the Yarkovsky effect, and the enhancement in collisional activity during its massive primordial phase (*O'Brien and Greenberg,* 2005; *Bottke et al.,* 2005a,b). In particular, *Bottke et al.* (2005a) explicitly incorporate the results of dynamical simulations of the excitation and clearing of the main belt by embedded planetary embryos performed by *Petit et al.* (2001). Such collisional/dynamical models can be constrained by a wide range of observational evidence such as the main-belt size distribution, the number of observed asteroid families, the existence of Vesta's basaltic crust, and the cosmic-ray exposure ages of ordinary chondrite meteorites, which suggest that the lifetimes of meter-scale stony bodies in the asteroid belt are on the order of 10–20 m.y. (*Marti and Graf,* 1992).

One of the most significant implications of having an early massive main belt, which was noted in early collisional models (e.g., *Chapman and Davis,* 1975) and recently emphasized in the case of collisional evolution plus dynamical depletion (e.g., *Bottke et al.,* 2005b), is that the majority of the collisional evolution of the asteroid belt occurred during its early, massive phase, and there has been relatively little change in the main-belt size distribution since then. The current, wavy main-belt size distribution, then, is a "fossil" from its first few hundred million years of collisional and dynamical evolution.

So how does the Kuiper belt compare to the asteroid belt in terms of its collisional and dynamical evolution? Evidence and modeling for the asteroid belt suggest that dynamical depletion, rather than collisional erosion, was primarily responsible for reducing the mass of the primordial asteroid belt to its current level. In the case of the Kuiper belt, this is less clear. As shown in section 3, collisional erosion, especially when aided by stellar perturbations or the formation of Neptune, can be very effective in removing mass. At the same time, dynamical models such as the Nice model result in the depletion of a large amount of mass through purely dynamical means and are able to match many observational constraints. Recent modeling that couples both collisional fragmentation and dynamical effects suggests that collisional erosion cannot play too large a role in removing mass from the Kuiper belt, otherwise the scattered disk and Oort cloud would be too depleted to explain the observed numbers of short- and long-period comets (*Charnoz and Morbidelli,* 2007). That model currently does not include coagulation. Further modeling work, which self-consistently integrates coagulation, collisional fragmentation, and dynamical effects, is necessary to fully constrain the relative contributions of collisional and dynamical depletion in the Kuiper belt.

We have noted that the asteroid belt has a collisionally relaxed size distribution that is not well-represented by a single power law over all size ranges. Should we expect the same for the Kuiper belt size distribution, and is there evidence to support this? The collision rate in the Kuiper belt should be roughly comparable to that in the asteroid belt, with the larger number of KBOs offsetting their lower intrinsic collision probability (*Davis and Farinella,* 1997), and as noted earlier in this chapter, the primordial Kuiper belt, like the asteroid belt, would have been substantially more massive than the current population. This suggests that the Kuiper belt should have experienced a degree of collisional evolution roughly comparable to the asteroid belt, and thus is likely to be collisionally relaxed like the asteroid belt. Observational evidence thus far is not detailed enough to say for sure if this is the case, although recent work (*Kenyon and Bromley,* 2004d; *Pan and Sari,* 2005) suggests that the observational estimate of the TNO size distribution by *Bernstein et al.* (2004), shown in Fig. 9, is consistent with a collisionally relaxed population.

While the Kuiper belt is likely to be collisionally relaxed, it is unlikely to mirror the exact shape of the asteroid belt size distribution. The shape of the size distribution is determined, in part, by the strength law Q_D^*, which is likely to differ somewhat between asteroids and KBOs. This is due to the difference in composition between asteroids, which are primarily rock, and KBOs, which contain a substantial amount of ice, as well as the difference in collision velocity between the two populations. With a mean velocity of ~5 km/s (*Bottke et al.,* 1994), collisions between asteroids are well into the supersonic regime (relative to the sound speed in rock). For the Kuiper belt, collision velocities are about a factor of 5 or more smaller (*Davis and Farinella,* 1997), such that collisions between KBOs are close to the subsonic/supersonic transition. For impacts occurring in these different velocity regimes, and into different materials, Q_D^* may differ significantly (e.g., *Benz and Asphaug,* 1999).

The difference in collision velocity can influence the size distribution in another way as well. With a mean collision velocity of ~5 km/s, a body of a given size in the asteroid belt can collisionally disrupt a significantly larger body. Thus, transitions in the strength properties of asteroids can lead to the formation of waves that propagate to larger sizes and manifest themselves as changes in the slope of the size distribution, as seen in Fig. 9. For the Kuiper belt, with collision velocities that are about a factor of 5 or more smaller than in the asteroid belt, the difference in size between a given body and the largest body it is capable of disrupting is much smaller than in the asteroid belt, and waves should therefore be much less pronounced or nonexistent in the KBO size distribution (e.g., *O'Brien and Greenberg,* 2003). There is still likely to be a change in slope at the largest sizes where the population transitions from being primordial to being collisionally relaxed, and such a change appears in the debiased observational data of *Bernstein et al.* (2004) (shown here in Fig. 9), although recent observations suggest that the change in slope may actually occur at smaller magnitudes than found in that survey (*Petit et al.,* 2006).

Is the size distribution of the Kuiper belt likely to be a "fossil" like the asteroid belt? The primordial Kuiper belt would have been substantially more massive than the current population. Thus, regardless of whether the depletion of its mass was primarily collisional or dynamical, collisional evolution would have been more intense early on and the majority of the collisional evolution would have occurred early in its history. In either case, its current size distribution could then be considered a fossil from that early phase, although defining exactly when that early phase ends and the size distribution becomes "fossilized" is not equally clear in both cases. In the case where the mass depletion of the Kuiper belt occurs entirely through collisions, there would not necessarily be a well-defined point at which one could say that the size distribution became fossilized, as the collision rate would decay continuously with time. In the case of dynamical depletion, where the mass would be removed fairly rapidly as in the case of the Nice model described in section 3.4, the collision rate would experience a correspondingly rapid drop, and the size distribution could be considered essentially fossilized after the dynamical depletion event.

As noted earlier in this section, an important observable manifestation of collisions in the asteroid belt is the formation of families, i.e., groupings of asteroids with similar orbits. Asteroid families are thought to be the fragments of collisionally disrupted parent bodies. These were first recognized by *Hirayama* (1918), who found 3 families among the 790 asteroids known at that time. The number increased to 7 families by 1926 when there were 1025 known asteroids (*Hirayama,* 1927). Today, there are over 350,000 known asteroids while the number of asteroid families has grown to about 30.

Given that the Kuiper belt is likely a collisionally evolved population, are there collisional families to be found among these bodies? Families are expected to be more difficult to recognize in the Kuiper belt than in the asteroid belt. Families are identified by finding statistically significant clusters of asteroid orbit elements — mainly the semimajor axis, eccentricity, and inclination. The collisional disruption of a parent body launches fragments with speeds of perhaps a few hundred meters per second relative to the original target body. This ejection speed is small compared with the orbital speeds of asteroids, hence the orbits of fragments differ by only small amounts from that of the original target body and, more importantly, from each other. Thus, the resulting clusters of fragments are easy to identify.

However, in the Kuiper belt, where ejection velocities are likely to be about the same but orbital speeds are much lower, collisional disruption produces a much greater dispersion in the orbital elements of fragments. This reduces the density of the clustering of orbital elements and makes the task of distinguishing family members from the background population much more difficult (*Davis and Farinella,* 1997). To date, there are over 1000 known KBOs, many of which have poorly determined orbits or are in resonances that would make the identification of a family difficult or impossible. *Chiang et al.* (2003) applied lowest-order secular theory to 227 nonresonant KBOs with well-determined orbits and found no convincing evidence for a dynamical family. Recently, however, *Brown et al.* (2007) found evidence for a single family with at least five members associated with KBO 2003 EL_{61}. This family was identified based on the unique spectroscopic signature of its members, and confirmed by their clustered orbit elements.

Given the small numbers involved, it cannot be said whether or not finding a single KBO family at this stage is statistically that different from the original identification of 3 asteroid families when there were only 790 known asteroids (*Hirayama,* 1918). However, the fact that the KBO family associated with 2003 EL_{61} was first discovered spectroscopically, and its clustering in orbital elements was later confirmed, while nearly all asteroid families were discovered based on clusterings in orbital elements alone, suggests that even if comparable numbers of KBO families and asteroid families do exist, the greater dispersion of KBO families in orbital element space may make them more difficult to identify unless there are spectroscopic signatures connecting them as well.

Perhaps when the number of nonresonant KBOs with good orbits approaches 1000, more populous Kuiper belt families will be identified, and as can be done now with the asteroid belt, these KBO families can be used as constraints on the interior structures of their original parent bodies as well as on the collisional and dynamical history of the Kuiper belt as a whole.

6. CONCLUDING REMARKS

Starting with a swarm of 1-m to 1-km planetesimals at 20–150 AU, the growth of icy planets follows a standard pattern (*Stern and Colwell,* 1997a,b; *Kenyon and Luu,* 1998, 1999a,b; *Kenyon and Bromley,* 2004a,d, 2005). Collisional damping and dynamical friction lead to a short period of runaway growth that produces 10–100 objects with r ~ 300–1000 km. As these objects grow, they stir the orbits of leftover planetesimals up to the disruption velocity. Once disruptions begin, the collisional cascade grinds leftover planetesimals into smaller objects faster than the oligarchs can accrete them. Thus, the oligarchs always contain a small fraction of the initial mass in solid material. For self-stirring models, oligarchs contain ~10% of the initial mass. Stellar flybys and stirring by a nearby gas giant augment the collisional cascade and leave less mass in oligarchs. The two examples in section 3.3 suggest that a very close flyby and stirring by Neptune leave ~2% to 5% of the initial mass in oligarchs with r ~ 100–1000 km.

This evolution differs markedly from planetary growth in the inner solar system. In ~0.1–1 m.y. at a few AU, runaway growth produces massive oligarchs, $m \geq 0.01\ M_{\oplus}$, that contain most of the initial solid mass in the disk. Aside from a few giant impacts like those that might produce the Moon (*Hartmann and Davis,* 1975; *Cameron and Ward,* 1976), collisions remove little mass from these objects. Although the collisional cascade removes many leftover planetesimals before oligarchs can accrete them, the lost material is much less than half the original solid mass (*Wetherill and Stewart,* 1993; *Kenyon and Bromley,* 2004b). For $a \geq 40$ AU, runaway growth leaves most of the mass in 0.1–10-km objects that are easily disrupted at modest collision velocities. In 4.5 G.y., the collisional cascade removes most of the initial disk mass inside 70–80 AU.

Together with numerical calculations of orbital dynamics (see chapter by Morbidelli et al.), theory now gives us a foundation for understanding the origin and evolution of the Kuiper belt. Within a disk of planetesimals at 20–100 AU, collisional growth naturally produces objects with r ~ 10–2000 km and a size distribution reasonably close to that observed among KBOs. As KBOs form, migration of the giant planets scatters KBOs into several dynamical classes (see chapter by Morbidelli et al.). Once the giant planets achieve their current orbits, the collisional cascade reduces the total mass in KBOs to current levels and produces the break in the size distribution at r ~ 20–40 km. Continued dynamical scattering by the giant planets sculpts the inner Kuiper belt and maintains the scattered disk.

New observations will allow us to test and to refine this theoretical picture. Aside from better measures of α_m, r_{max}, and r_0 among the dynamical classes, better limits on the total mass and the size distribution of large KBOs with a ~ 50–100 AU should yield a clear discriminant among theoretical models. In the Nice model, the Kuiper belt was initially nearly empty outside ~50 AU. Thus, any KBOs found with a ~ 50–100 AU should have the collisional and dynamical signatures of the scattered disk or detached population. If some KBOs formed *in situ* at a ≥ 50 AU, their size distribution depends on collisional growth modified by self-stirring and stirring by ~30 $M_\oplus$ of large KBOs formed at 20–30 AU and scattered through the Kuiper belt by the giant planets. From the calculations of Neptune stirring (section 3.3), stirring by scattered disk objects should yield a size distribution markedly different from the size distribution of detached or scattered disk objects formed at 20–30 AU. Wide-angle surveys on 2–3-m-class telescopes (e.g., Pan-Starrs) and deep probes with 8–10-m telescopes can provide this test.

Information on smaller size scales — α_d and r_1 — place additional constraints on the bulk properties (fragmentation parameters) of KBOs and on the collisional cascade. In any of the stirring models, there is a strong correlation between r_0, r_1, and the fragmentation parameters. Thus, direct measures of r_0 and r_1 provide a clear test of KBO formation calculations. At smaller sizes (r ≤ 0.1 km), the slope of the size distribution α_d clearly tests the fragmentation algorithm and the ability of the collisional cascade to remove KBOs with r ~ 1–10 km. Although the recent detection of KBOs with r ≪ 1 km (*Chang et al.,* 2006) may be an instrumental artifact (*Jones et al.,* 2006; *Chang et al.,* 2007), optical and X-ray occultations (e.g., TAOS) will eventually yield these tests.

Finally, there is a clear need to combine coagulation and dynamical calculations to produce a "unified" picture of planet formation at a ≥ 20 AU. *Charnoz and Morbidelli* (2007) provide a good start in this direction. Because the collisional outcome is sensitive to internal *and* external dynamics, understanding the formation of the observed n(r), n(e), and n(i) distributions in each KBO population requires treating collisional evolution and dynamics together. A combined approach should yield the sensitivity of α_m, r_{max}, and r_0 to the local evolution and the timing of the formation of giant planets, Neptune migration, and stellar flybys. These calculations will also test how the dynamical events depend on the evolution during oligarchic growth and the collisional cascade. Coupled with new observations of KBOs and of planets and debris disks in other planetary systems, these calculations should give us a better understanding of the origin and evolution of KBOs and other objects in the outer solar system.

Acknowledgments. We thank S. Charnoz, S. Kortenkamp, A. Morbidelli, and an anonymous reviewer for comments that considerably improved the text. We acknowledge support from the NASA Astrophysics Theory Program (grant NAG5-13278. B.C.B. and S.J.K.), the NASA Planetary Geology and Geophysics Program (grant NNX06AC50G, D.P.O.), and the JPL Institutional Computing and Information Services and the NASA Directorates of Aeronautics Research, Science, Exploration Systems, and Space Operations (B.C.B. and S.J.K.). This paper is PSI Contribution 417.

REFERENCES

Adachi I., Hayashi C., and Nakazawa K. (1976) The gas drag effect on the elliptical motion of a solid body in the primordial solar nebula. *Progr. Theor. Phys., 56,* 1756–1771.

Adams F. C. and Laughlin G. (2001) Constraints on the birth aggregate of the solar system. *Icarus, 150,* 151–162.

Artymowicz P. (1988) Radiation pressure forces on particles in the Beta Pictoris system. *Astrophys. J. Lett., 335,* L79–L82.

Artymowicz P. (1997) Beta Pictoris: An early solar system? *Annu. Rev. Earth Planet. Sci., 25,* 175–219.

Asphaug E. (1997) Impact origin of the Vesta family. *Meteoritics & Planet. Sci., 32,* 965–980.

Asphaug E. and Benz W. (1996) Size, density, and structure of Comet Shoemaker-Levy 9 inferred from the physics of tidal breakup. *Icarus, 121,* 225–248.

Aumann H. H., Beichman C. A., Gillett F. C., de Jong T., Houck J. R., Low F. J., Neugebauer G., Walker R. G., and Wesselius P. R. (1984) Discovery of a shell around Alpha Lyrae. *Astrophys. J. Lett., 278,* L23–L27.

Backman D. E. and Paresce F. (1993) Main-sequence stars with circumstellar solid material — The VEGA phenomenon. In *Protostars and Planets III* (E. H. Levy and J. I. Lunine, eds.), pp. 1253–1304. Univ. of Arizona, Tucson.

Beckwith S. V. W. and Sargent A. I. (1996) Circumstellar disks and the search for neighbouring planetary systems. *Nature, 383,* 139–144.

Benz W. and Asphaug E. (1999) Catastrophic disruptions revisited. *Icarus, 142,* 5–20.

Bernstein G. M., Trilling D. E., Allen R. L., Brown M. E., Holman M., and Malhotra R. (2004) The size distribution of trans-neptunian bodies. *Astron. J., 128,* 1364–1390.

Bottke W. F., Nolan M. C., Greenberg R., and Kolvoord R. A. (1994) Velocity distributions among colliding asteroids. *Icarus, 107,* 255–268.

Bottke W. F., Durda D. D., Nesvorný D., Jedicke R., Morbidelli A., Vokrouhlický D., and Levison H. F. (2005a) Linking the collisional history of the main asteroid belt to its dynamical excitation and depletion. *Icarus, 179,* 63–94.

Bottke W. F., Durda D. D., Nesvorný D., Jedicke R., Morbidelli A., Vokrouhlický D., and Levison H. (2005b) The fossilized size distribution of the main asteroid belt. *Icarus, 175,* 111–140.

Bromley B. C. and Kenyon S. J. (2006) A hybrid N-body-coagulation code for planet formation. *Astron. J., 131,* 2737–2748.

Brown M. E., Barkume K. M., Ragozzine D., and Scahller E. L. (2007) A collisional family of icy objects in the Kuiper belt. *Nature, 446,* 294–297.

Burns J. A., Lamy P. L., and Soter S. (1979) Radiation forces on small particles in the solar system. *Icarus, 40,* 1–48.

Cameron A. G. W. and Ward W. R. (1976) The origin of the Moon (abstract). In *Lunar Science VII,* pp. 120–121. The Lunar Science Institute, Houston.

Campo Bagatin A., Farinella P., and Paolicchi P. (1993) Collisional evolution of the asteroid size distribution: A numerical simulation. *Cel. Mech. Dyn. Astron., 57,* 403–404.

Campo Bagatin A., Cellino A., Davis D. R., Farinella P., and Paolicchi P. (1994) Wavy size distributions for collisional systems with a small-size cutoff. *Planet. Space Sci., 42,* 1079–1092.

Campo Bagatin A., Petit J.-M., and Farinella P. (2001) How many rubble piles are in the asteroid belt? *Icarus, 149,* 198–209.

Chang H.-K., King S.-K., Liang J.-S., Wu P.-S., Lin L. C.-C., and Chiu J.-L. (2006) Occultation of X-rays from Scorpius X-1 by small trans-neptunian objects. *Nature, 442,* 660–663.

Chang H.-K., Liang J.-S., Liu C.-Y., and King S.-K. (2007) Millisecond dips in the RXTE/PCA light curve of Sco X-1 and TNO occultation. *Mon. Not. R. Astron. Soc., 378,* 1287.

Chapman C. R. and Davis D. R. (1975) Asteroid collisional evolution — Evidence for a much larger early population. *Science, 190,* 553–556.

Charnoz S. and Morbidelli A. (2007) Coupling dynamical and collisional evolution of small bodies II: Forming the Kuiper belt, the scattered disk and the Oort cloud. *Icarus, 188,* 468–480.

Charnoz S., Thébault P., and Brahic A. (2001) Short-term collisional evolution of a disc perturbed by a giant-planet embryo. *Astron. Astrophys., 373,* 683–701.

Chiang E. I., Lovering J. R., Millis R. L., Buie M. W., Wasserman L. H., and Meech K. J. (2003) Resonant and secular families of the Kuiper belt. *Earth Moon Planets, 92,* 49–62.

Chiang E., Lithwick Y., Murray-Clay R., Buie M., Grundy W., and Holman M. (2007) A brief history of transneptunian space. In *Protostars and Planets V* (B. Reipurth et al., eds.), pp. 895–911. Univ. of Arizona, Tucson.

Davis D. R. and Farinella P. (1997) Collisional evolution of Edgeworth-Kuiper belt objects. *Icarus, 125,* 50–60.

Davis D. R., Chapman C. R., Greenberg R., Weidenschilling S. J., and Harris A. W. (1979) Collisional evolution of asteroids — Populations, rotations, and velocities. In *Asteroids* (T. Gehrels, ed.), pp. 528–557. Univ. of Arizon, Tucson.

Davis D. R., Chapman C. R., Weidenschilling S. J., and Greenberg R. (1985) Collisional history of asteroids: Evidence from Vesta and the Hirayama families. *Icarus, 63,* 30–53.

Davis D. R., Weidenschilling S. J., Farinella P., Paolicchi P., and Binzel R. P. (1989) Asteroid collisional history — Effects on sizes and spins. In *Asteroids II* (R. P. Binzel et al., eds.), pp. 805–826. Univ. of Arizona, Tucson.

Davis D. R., Ryan E. V., and Farinella P. (1994) Asteroid collisional evolution: Results from current scaling algorithms. *Planet. Space Sci., 42,* 599–610.

Davis D. R., Farinella P., and Weidenschilling S. J. (1999) Accretion of a massive Edgeworth-Kuiper belt (abstract). In *Lunar and Planetary Science XXX,* pp. 1883–1884. Lunar and Planetary Institute, Houston.

de la Fuente Marcos C. and Barge P. (2001) The effect of long-lived vortical circulation on the dynamics of dust particles in the mid-plane of a protoplanetary disc. *Mon. Not. R. Astron. Soc., 323,* 601–614.

Dohnanyi J.W. (1969) Collisional models of asteroids and their debris. *J. Geophys. Res., 74,* 2531–2554.

Dullemond C. P. and Dominik C. (2005) Dust coagulation in protoplanetary disks: A rapid depletion of small grains. *Astron. Astrophys., 434,* 971–986.

Duncan M. (1994) Orbital stability and the structure of the solar system. In *Circumstellar Dust Disks and Planet Formation* (R. Ferlet and A. Vidal-Madjar, eds.), pp. 245–255. Editions Frontieres, Gif-sûr-Yvette.

Duncan M. J. and Levison H. F. (1997) A scattered comet disk and the origin of Jupiter family comets. *Science, 276,* 1670–1672.

Duncan M. J., Levison H. F., and Budd S. M. (1995) The dynamical structure of the Kuiper belt. *Astron. J., 110,* 3073–3081.

Durda D. D. (1993) The collisional evolution of the asteroid belt and its contribution to the zodiacal cloud. Ph.D. Thesis, Univ. of Florida.

Durda D. D. and Dermott S. F. (1997) The collisional evolution of the asteroid belt and its contribution to the zodiacal cloud. *Icarus, 130,* 140–164.

Durda D. D., Greenberg R., and Jedicke R. (1998) Collisional models and scaling laws: A new interpretation of the shape of the main-belt asteroid size distribution. *Icarus, 135,* 431–440.

Elliot J. L., Kern S. D., Clancy K. B., Gulbis A. A. S., Millis R. L., Buie M. W., Wasserman L. H., Chiang E. I., Jordan A. B., Trilling D. E., and Meech K. J. (2005) The Deep Ecliptic Survey: A search for Kuiper belt objects and Centaurs. II. Dynamical classification, the Kuiper belt plane, and the core population. *Astron. J., 129,* 1117–1162.

Giblin I., Davis D. R., and Ryan E. V. (2004) On the collisional disruption of porous icy targets simulating Kuiper belt objects. *Icarus, 171,* 487–505.

Gladman B., Kavelaars J. J., Petit J., Morbidelli A., Holman M. J., and Loredo T. (2001) The structure of the Kuiper belt: Size distribution and radial extent. *Astron. J., 122,* 1051–1066.

Gladman B. J., Davis D. R., Neese N., Williams G., Jedicke R., Kavelaars J. J., Petit J.-M., Scholl H., Holman M., Warrington B., Esquerdo G., and Tricarico P. (2007) SKADS: A Sub-Kilometer Asteroid Diameter Survey. *Icarus,* in press.

Goldreich P. and Ward W. R. (1973) The formation of planetesimals. *Astrophys. J., 183,* 1051–1062.

Goldreich P., Lithwick Y., and Sari R. (2004) Planet formation by coagulation: A focus on Uranus and Neptune. *Annu. Rev. Astron. Astrophys., 42,* 549–601.

Gomes R., Levison H. F., Tsiganis K., and Morbidelli A. (2005) Origin of the cataclysmic late heavy bombardment period of the terrestrial planets. *Nature, 435,* 466–469.

Gomez M., Hartmann L., Kenyon S. J., and Hewett R. (1993) On the spatial distribution of pre-main-sequence stars in Taurus. *Astron. J., 105,* 1927–1937.

Gradie J. and Tedesco E. (1982) Compositional structure of the asteroid belt. *Science, 216,* 1405–1407.

Greaves J. S. (2005) Disks around stars and the growth of planetary systems. *Science, 307,* 68–71.

Greaves J. S., Holland W. S., Moriarty-Schieven G., Jenness T., Dent W. R. F., Zuckerman B., McCarthy C., Webb R. A., Butner H. M., Gear W. K., and Walker H. J. (1998) A dust ring around epsilon Eridani: Analog to the young solar system. *Astrophys. J. Lett., 506,* L133–L137.

Greaves J. S., Wyatt M. C., Holland W. S., and Dent W. R. F. (2004) The debris disc around τ Ceti: A massive analogue to the Kuiper belt. *Mon. Not. R. Astron. Soc., 351,* L54–L58.

Greenberg R., Hartmann W. K., Chapman C. R., and Wacker J. F. (1978) Planetesimals to planets — Numerical simulation of collisional evolution. *Icarus, 35,* 1–26.

Greenberg R., Weidenschilling S. J., Chapman C. R., and Davis D. R. (1984) From icy planetesimals to outer planets and comets. *Icarus, 59,* 87–113.

Greenzweig Y. and Lissauer J. J. (1990) Accretion rates of protoplanets. *Icarus, 87,* 40–77.

Haisch K. E. Jr., Lada E. A., and Lada C. J. (2001) Disk frequencies and lifetimes in young clusters. *Astrophys. J. Lett., 553,* L153–L156.

Hartmann W. K. and Davis D. R. (1975) Satellite-sized planetesimals and lunar origin. *Icarus, 24,* 504–514.

Hayashi C. (1981) Structure of the solar nebula, growth and decay of magnetic fields and effects of magnetic and turbulent viscosities on the nebula. *Progr. Theor. Phys. Suppl., 70,* 35–53.

Heppenheimer T. A. (1980) Secular resonances and the origin of eccentricities of Mars and the asteroids. *Icarus, 41,* 76–88.

Hirayama K. (1918) Groups of asteroids probably of common origin. *Astron. J., 31,* 185–188.

Hirayama K. (1927) Families of asteroids: Second paper. *Ann. Observ. Astron. Tokyo, 19,* 1–26.

Holman M. J. and Wisdom J. (1993) Dynamical stability in the outer solar system and the delivery of short period comets. *Astron. J., 105,* 1987–1999.

Holsapple K. A. (1994) Catastrophic disruptions and cratering of solar system bodies: A review and new results. *Planet. Space Sci., 42,* 1067–1078.

Hornung P., Pellat R., and Barge P. (1985) Thermal velocity equilibrium in the protoplanetary cloud. *Icarus, 64,* 295–307.

Housen K. R. and Holsapple K. A. (1990) On the fragmentation of asteroids and planetary satellites. *Icarus, 84,* 226–253.

Housen K. R. and Holsapple K. A. (1999) Scale effects in strength-dominated collisions of rocky asteroids. *Icarus, 142,* 21–33.

Ida S., Larwood J., and Burkert A. (2000) Evidence for early stellar encounters in the orbital distribution of Edgeworth-Kuiper belt objects. *Astrophys. J., 528,* 351–356.

Inaba S. and Barge P. (2006) Dusty vortices in protoplanetary disks. *Astrophys. J., 649,* 415–427.

Ivezić Ž., Tabachnik S., Rafikov R., Lupton R. H., Quinn T., Hammergren M., Eyer L., Chu J., Armstrong J. C., Fan X., Finlator K., Geballe T. R., Gunn J. E., Hennessy G. S., Knapp G. R., Leggett S. K., Munn J. A., Pier J. R., Rockosi C. M., Schneider D. P., Strauss M. A., Yanny B., Brinkmann J., Csabai I., Hindsley R. B., Kent S., Lamb D. Q., Margon B., McKay T. A., Smith J. A., Waddel P., York D. G., and the SDSS Collaboration (2001) Solar system objects observed in the Sloan Digital Sky Survey commissioning data. *Astron. J., 122,* 2749–2784.

Jedicke R. and Metcalfe T. S. (1998) The orbital and absolute magnitude distributions of main belt asteroids. *Icarus, 131,* 245–260.

Jones T. A., Levine A. M., Morgan E. H., and Rappaport S. (2006) Millisecond dips in Sco X-1 are likely the result of high-energy particle events. *The Astronomer's Telegram, 949.*

Kenyon S. J. and Bromley B. C. (2002a) Collisional cascades in planetesimal disks. I. Stellar flybys. *Astron. J., 123,* 1757–1775.

Kenyon S. J. and Bromley B. C. (2002b) Dusty rings: Signposts of recent planet formation. *Astrophys. J. Lett., 577,* L35–L38.

Kenyon S. J. and Bromley B. C. (2004a) Collisional cascades in planetesimal disks. II. Embedded planets. *Astron. J., 127,* 513–530.

Kenyon S. J. and Bromley B. C. (2004b) Detecting the dusty debris of terrestrial planet formation. *Astrophys. J. Lett., 602,* L133–L136.

Kenyon S. J. and Bromley B. C. (2004c) Stellar encounters as the origin of distant solar system objects in highly eccentric orbits. *Nature, 432,* 598–602.

Kenyon S. J. and Bromley B. C. (2004d) The size distribution of Kuiper belt objects. *Astron. J., 128,* 1916–1926.

Kenyon S. J. and Bromley B. C. (2005) Prospects for detection of catastrophic collisions in debris disks. *Astron. J., 130,* 269–279.

Kenyon S. J. and Bromley B. C. (2006) Terrestrial planet formation. I. The transition from oligarchic growth to chaotic growth. *Astron. J., 131,* 1837–1850.

Kenyon S. J. and Hartmann L. (1987) Spectral energy distributions of T Tauri stars — Disk flaring and limits on accretion. *Astrophys. J., 323,* 714–733.

Kenyon S. J. and Luu J. X. (1998) Accretion in the early Kuiper belt. I. Coagulation and velocity evolution. *Astron. J., 115,* 2136–2160.

Kenyon S. J. and Luu J. X. (1999a) Accretion in the early Kuiper belt. II. Fragmentation. *Astron. J., 118,* 1101–1119.

Kenyon S. J. and Luu J. X. (1999b) Accretion in the early outer solar system. *Astrophys. J., 526,* 465–470.

Knežević Z. and Milani A. (2003) Proper element catalogs and asteroid families. *Astron. Astrophys., 403,* 1165–1173.

Kobayashi H., Ida S., and Tanaka H. (2005) The evidence of an early stellar encounter in Edgeworth Kuiper belt. *Icarus, 177,* 246–255.

Kokubo E. and Ida S. (1995) Orbital evolution of protoplanets embedded in a swarm of planetesimals. *Icarus, 114,* 247–257.

Kokubo E. and Ida S. (1998) Oligarchic growth of protoplanets. *Icarus, 131,* 171–178.

Kokubo E. and Ida S. (2000) Formation of protoplanets from planetesimals in the solar nebula. *Icarus, 143,* 15–27.

Kokubo E. and Ida S. (2002) Formation of protoplanet systems and diversity of planetary systems. *Astrophys. J., 581,* 666–680.

Krivov A. V., Löhne T., and Sremčević M. (2006) Dust distributions in debris disks: Effects of gravity, radiation pressure and collisions. *Astron. Astrophys., 455,* 509–519.

Kuchner M. J., Brown M. E., and Holman M. (2002) Long-term dynamics and the orbital inclinations of the classical Kuiper belt objects. *Astron. J., 124,* 1221–1230.

Lada C. J. (2006) Stellar multiplicity and the initial mass function: Most stars are single. *Astrophys. J. Lett., 640,* L63–L66.

Lada C. J. and Lada E. A. (2003) Embedded clusters in molecular clouds. *Annu. Rev. Astron. Astrophys., 41,* 57–115.

Landgraf M., Liou J.-C., Zook H. A., and Grün E. (2002) Origins of solar system dust beyond Jupiter. *Astron. J., 123,* 2857–2861.

Lecar M. and Franklin F. A. (1973) On the original distribution of the asteroids I. *Icarus, 20,* 422–436.

Lecar M. and Franklin F. A. (1997) The solar nebula, secular resonances, gas drag, and the asteroid belt. *Icarus, 129,* 134–146.

Lee M. H. (2000) On the validity of the coagulation equation and the nature of runaway growth. *Icarus, 143,* 74–86.

Leinhardt Z. M. and Richardson D. C. (2002) N-body simulations of planetesimal evolution: Effect of varying impactor mass ratio. *Icarus, 159,* 306–313.

Leinhardt Z. M. and Richardson D. C. (2005) Planetesimals to protoplanets. I. Effect of fragmentation on terrestrial planet formation. *Astrophys. J., 625,* 427–440.

Lemaitre A. and Dubru P. (1991) Secular resonances in the primitive solar nebula. *Cel. Mech. Dyn. Astron., 52,* 57–78.

Levison H. F. and Duncan M. J. (1990) A search for proto-comets in the outer regions of the solar system. *Astron. J., 100,* 1669–1675.

Levison H. F. and Morbidelli A. (2007) Models of the collisional damping scenario for ice giant planets and Kuiper belt formation. *Icarus, 189,* 196–212.

Levison H. F. and Stern S. A. (2001) On the size dependence of the inclination distribution of the main Kuiper belt. *Astron. J., 121,* 1730–1735.

Levison H. F., Morbidelli A., and Dones L. (2004) Sculpting the Kuiper belt by a stellar encounter: Constraints from the Oort cloud and scattered disk. *Astron. J., 128,* 2553–2563.

Lissauer J. J. (1987) Timescales for planetary accretion and the structure of the protoplanetary disk. *Icarus, 69,* 249–265.

Luhman K. L. (2006) The spatial distribution of brown dwarfs in Taurus. *Astrophys. J., 645,* 676–687.

Luu J. X. and Jewitt D. C. (2002) Kuiper belt objects: Relics from the accretion disk of the Sun. *Annu. Rev. Astron. Astrophys., 40,* 63–101.

Malhotra R. (1995) The origin of Pluto's orbit: Implications for the solar system beyond Neptune. *Astron. J., 110,* 420–429.

Malhotra R. (1996) The phase space structure near Neptune resonances in the Kuiper belt. *Astron. J., 111,* 504–516.

Malyshkin L. and Goodman J. (2001) The timescale of runaway stochastic coagulation. *Icarus, 150,* 314–322.

Marti K. and Graf T. (1992) Cosmic-ray exposure history of ordinary chondrites. *Annu. Rev. Earth Planet. Sci., 20,* 221–243.

Marzari F., Cellino A., Davis D. R., Farinella P., Zappala V., and Vanzani V. (1996) Origin and evolution of the Vesta asteroid family. *Astron. Astrophys., 316,* 248–262.

Marzari F., Farinella P., and Davis D. R. (1999) Origin, aging, and death of asteroid families. *Icarus, 142,* 63–77.

McCord T. B., Adams J. B., and Johnson T. V. (1970) Asteroid Vesta: Spectral reflectivity and compositional implications. *Science, 178,* 745–747.

Michel P., Benz W., Tanga P., and Richardson D. C. (2001) Collisions and gravitational reaccumulation: Forming asteroid families and satellites. *Science, 294,* 1696–1700.

Morbidelli A. and Levison H. F. (2004) Scenarios for the origin of the orbits of the trans-neptunian objects 2000 CR_{105} and 2003 VB_{12} (Sedna). *Astron. J., 128,* 2564–2576.

Morbidelli A., Jacob C., and Petit J.-M. (2002) Planetary embryos never formed in the Kuiper belt. *Icarus, 157,* 241–248.

Morbidelli A., Emel'yanenko V. V., and Levison H. F. (2004) Origin and orbital distribution of the trans-neptunian scattered disc. *Mon. Not. R. Astron. Soc., 355,* 935–940.

Morbidelli A., Levison H. F., Tsiganis K., and Gomes R. (2005) Chaotic capture of Jupiter's Trojan asteroids in the early solar system. *Nature, 435,* 462–465.

Nagasawa M. and Ida S. (2000) Sweeping secular resonances in the Kuiper belt caused by depletion of the solar nebula. *Astron. J., 120,* 3311–3322.

Nagasawa M., Tanaka H., and Ida S. (2000) Orbital evolution of asteroids during depletion of the solar nebula. *Astron. J., 119,* 1480–1497.

Nagasawa M., Ida S., and Tanaka H. (2001) Origin of high orbital eccentricity and inclination of asteroids. *Earth Planets Space, 53,* 1085–1091.

Nagasawa M., Ida S., and Tanaka H. (2002) Excitation of orbital inclinations of asteroids during depletion of a protoplanetary disk: Dependence on the disk configuration. *Icarus, 159,* 322–327.

Nagasawa M., Lin D. N. C., and Thommes E. (2005) Dynamical shake-up of planetary systems. I. Embryo trapping and induced collisions by the sweeping secular resonance and embryo-disk tidal interaction. *Astrophys. J., 635,* 578–598.

Natta A., Grinin V., and Mannings V. (2000) Properties and evolution of disks around pre-main-sequence stars of intermediate mass. In *Protostars and Planets IV* (V. Mannings et al., eds.), pp. 559–588. Univ. of Arizona, Tucson.

Null G. W., Owen W. M., and Synnott S. P. (1993) Masses and densities of Pluto and Charon. *Astron. J., 105,* 2319–2335.

O'Brien D. P. and Greenberg R. (2003) Steady-state size distributions for collisional populations: Analytical solution with size-dependent strength. *Icarus, 164,* 334–345.

O'Brien D. P. and Greenberg R. (2005) The collisional and dynamical evolution of the main-belt and NEA size distributions. *Icarus, 178,* 179–212.

O'Brien D. P., Morbidelli A., and Bottke W. F. (2005) Collisional evolution of the primordial trans-neptunian disk: Implications for planetary migration and the current size distribution of TNOs. *Bull. Am. Astron. Soc., 37,* 676.

O'Brien D. P., Morbidelli A., and Bottke W. F. (2007) Re-evaluating the primordial excitation and clearing of the asteroid belt. *Icarus, 191,* in press.

Ohtsuki K. (1992) Evolution of random velocities of planetesimals in the course of accretion. *Icarus, 98,* 20–27.

Ohtsuki K., Nakagawa Y., and Nakazawa K. (1990) Artificial acceleration in accumulation due to coarse mass-coordinate divisions in numerical simulation. *Icarus, 83,* 205–215.

Ohtsuki K., Stewart G. R., and Ida S. (2002) Evolution of planetesimal velocities based on three-body orbital integrations and growth of protoplanets. *Icarus, 155,* 436–453.

Pan M. and Sari R. (2005) Shaping the Kuiper belt size distribution by shattering large but strengthless bodies. *Icarus, 173,* 342–348.

Petit J., Morbidelli A., and Chambers J. (2001) The primordial excitation and clearing of the asteroid belt. *Icarus, 153,* 338–347.

Petit J., Chambers J., Franklin F., and Nagasawa M. (2002) Primordial excitation and depletion of the main belt. In *Asteroids III* (W. F. Bottke Jr. et al., eds.), pp. 711–738. Univ. of Arizona, Tucson.

Petit J.-M., Holman M. J., Gladman B. J., Kavelaars J. J., Scholl H., and Loredo T. J. (2006) The Kuiper Belt luminosity function from m_R = 22 to 25. *Mon. Not. R. Astron. Soc., 365,* 429–438.

Rafikov R. R. (2003a) Dynamical evolution of planetesimals in protoplanetary disks. *Astron. J., 126,* 2529–2548.

Rafikov R. R. (2003b) Planetesimal disk evolution driven by embryo-planetesimal gravitational scattering. *Astron. J., 125,* 922–941.

Rafikov R. R. (2003c) Planetesimal disk evolution driven by planetesimal-planetesimal gravitational scattering. *Astron. J., 125,* 906–921.

Rafikov R. R. (2003d) The growth of planetary embryos: Orderly, runaway, or oligarchic? *Astron. J., 125,* 942–961.

Ryan E. V., Davis D. R., and Giblin I. (1999) A laboratory impact study of simulated Edgeworth-Kuiper belt objects. *Icarus, 142,* 56–62.

Safronov V. S. (1969) *Evoliutsiia Doplanetnogo Oblaka (Evolution of the Protoplanetary Cloud and Formation of the Earth and Planets),* Nauka, Moscow. (Translated in 1972, NASA TT F-677.)

Safronov V. S. (1979) On the origin of asteroids. In *Asteroids* (T. Gehrels, ed.), pp. 975–991. Univ. of Arizona, Tucson.

Scholz A., Jayawardhana R., and Wood K. (2006) Exploring brown dwarf disks: A 1.3 mm survey in Taurus. *Astrophys. J., 645,* 1498–1508.

Slesnick C. L., Hillenbrand L. A., and Carpenter J. M. (2004) The spectroscopically determined substellar mass function of the Orion nebula cluster. *Astrophys. J., 610,* 1045–1063.

Spaute D., Weidenschilling S. J., Davis D. R., and Marzari F. (1991) Accretional evolution of a planetesimal swarm. I — A new simulation. *Icarus, 92,* 147–164.

Stern S. A. (1995) Collisional time scales in the Kuiper disk and their implications. *Astron. J., 110,* 856–868.

Stern S. A. (2005) Regarding the accretion of 2003 VB_{12} (Sedna) and like bodies in distant heliocentric orbits. *Astron. J., 129,* 526–529.

Stern S. A. and Colwell J. E. (1997a) Accretion in the Edgeworth-Kuiper belt: Forming 100–1000 km radius bodies at 30 AU and beyond. *Astron. J., 114,* 841–849.

Stern S. A. and Colwell J. E. (1997b) Collisional erosion in the primordial Edgeworth-Kuiper belt and the generation of the 30–50 AU Kuiper gap. *Astrophys. J., 490,* 879–882.

Takeuchi T. and Artymowicz P. (2001) Dust migration and morphology in optically thin circumstellar gas disks. *Astrophys. J., 557,* 990–1006.

Tanaka H. and Ida S. (1999) Growth of a migrating protoplanet. *Icarus, 139,* 350–366.

Tanga P., Weidenschilling S. J., Michel P., and Richardson D. C. (2004) Gravitational instability and clustering in a disk of planetesimals. *Astron. Astrophys., 427,* 1105–1115.

Thomas P. C., Binzel R. P., Gaffey M. J., Storrs A. D., Wells E. N., and Zellner B. H. (1997) Impact excavation on asteroid 4 Vesta: Hubble Space Telescope results. *Science, 277,* 1492–1495.

Thommes E. W., Duncan M. J., and Levison H. F. (1999) The formation of Uranus and Neptune in the Jupiter-Saturn region of the solar system. *Nature, 402,* 635–638.

Thommes E. W., Duncan M. J., and Levison H. F. (2002) The formation of Uranus and Neptune among Jupiter and Saturn. *Astron. J., 123,* 2862–2883.

Tsiganis K., Gomes R., Morbidelli A., and Levison H. F. (2005) Origin of the orbital architecture of the giant planets of the solar system. *Nature, 435,* 459–461.

Ward W. R. (1981) Solar nebula dispersal and the stability of the planetary system. I — Scanning secular resonance theory. *Icarus, 47,* 234–264.

Weidenschilling S. J. (1977a) Aerodynamics of solid bodies in the solar nebula. *Mon. Not. R. Astron. Soc., 180,* 57–70.

Weidenschilling S. J. (1977b) The distribution of mass in the planetary system and solar nebula. *Astrophys. Space Sci., 51,* 153–158.

Weidenschilling S. J. (1980) Dust to planetesimals — Settling and coagulation in the solar nebula. *Icarus, 44,* 172–189.

Weidenschilling S. J. (1984) Evolution of grains in a turbulent solar nebula. *Icarus, 60,* 553–567.

Weidenschilling S. J. (1989) Stirring of a planetesimal swarm — The role of distant encounters. *Icarus, 80,* 179–188.

Weidenschilling S. J. (1995) Can gravitation instability form planetesimals? *Icarus, 116,* 433–435.

Weidenschilling S. J. (2003) Radial drift of particles in the solar nebula: Implications for planetesimal formation. *Icarus, 165,* 438–442.

Weidenschilling S. J. (2006) Models of particle layers in the midplane of the solar nebula. *Icarus, 181,* 572–586.

Weidenschilling S. J., Spaute D., Davis D. R., Marzari F., and Ohtsuki K. (1997) Accretional evolution of a planetesimal swarm. *Icarus, 128,* 429–455.

Wetherill G. W. (1989) Origin of the asteroid belt. In *Asteroids II* (R. P. Binzel et al., eds.), pp. 661–680. Univ. of Arizona, Tucson.

Wetherill G. W. (1990) Comparison of analytical and physical modeling of planetesimal accumulation. *Icarus, 88,* 336–354.

Wetherill G. W. (1992) An alternative model for the formation of the asteroids. *Icarus, 100,* 307–325.

Wetherill G. W. and Stewart G. R. (1989) Accumulation of a swarm of small planetesimals. *Icarus, 77,* 330–357.

Wetherill G. W. and Stewart G. R. (1993) Formation of planetary embryos — Effects of fragmentation, low relative velocity, and independent variation of eccentricity and inclination. *Icarus, 106,* 190–209.

Williams D. R. and Wetherill G. W. (1994) Size distribution of collisionally evolved asteroidal populations — Analytical solution for self-similar collision cascades. *Icarus, 107,* 117–128.

Williams J. P., Najita J., Liu M. C., Bottinelli S., Carpenter J. M., Hillenbrand L. A., Meyer M. R., and Soderblom D. R. (2004) Detection of cool dust around the G2 V star HD 107146. *Astrophys. J., 604,* 414–419.

Wurm G. and Krauss O. (2006) Concentration and sorting of chondrules and CAIs in the late solar nebula. *Icarus, 180,* 487–495.

Wurm G., Paraskov G., and Krauss O. (2004) On the importance of gas flow through porous bodies for the formation of planetesimals. *Astrophys. J., 606,* 983–987.

Wyatt M. C., Greaves J. S., Dent W. R. F., and Coulson I. M. (2005) Submillimeter images of a dusty Kuiper belt around η Corvi. *Astrophys. J., 620,* 492–500.

Yoshida F., Nakamura T., Watanabe J., Kinoshita D., Yamamoto N., and Fuse T. (2003) Size and spatial distributions of sub-km main-belt asteroids. *Publ. Astron. Soc. Japan, 55,* 701–715.

Youdin A. N. and Shu F. H. (2002) Planetesimal formation by gravitational instability. *Astrophys. J., 580,* 494–505.